

Linear spectropolarimetry across the optical spectrum of Herbig Ae/Be stars^{*}

K. M. Ababakr^{1†}, R. D. Oudmaijer¹ and J.S. Vink²

¹*School of Physics and Astronomy, University of Leeds, EC Stoner Building, Leeds LS2 9JT, UK*

²*Armagh Observatory, College Hill, Armagh, UK*

Accepted 2016 June 22. Received 2016 June 22; in original form 2016 April 29

ABSTRACT

We present the results of spectropolarimetric observations of 12 Herbig Ae/Be objects. Our data have the largest spectropolarimetric wavelength coverage, 4560 Å to 9480 Å, published to date. A change in linear polarisation across the H α line, is detected in all objects. Such a line effect reveals the fact that stellar photons are scattered off free electrons that are not distributed in a spherically symmetric volume, suggesting the presence of small disks around these accreting objects. Thanks to the large wavelength coverage, we can report that H α is the spectral line in the optical wavelength range that is most sensitive to revealing deviations from spherical symmetry, and the one most likely to show a line effect across the polarisation in such cases. Few other spectral lines display changes in polarisation across the line. In addition, H α is the only line which shows an effect across its absorption component in some sources. We present a scenario explaining this finding and demonstrate that the detection of the line effect strongly relies on the number of photons scattered into our line of sight. We highlight the special case of R Mon, which is the only object in our sample to show many lines with a polarisation effect, which is much stronger than in all other objects. Given that the object and its nebulosity is spatially resolved, we argue that this is due to scattering of the stellar and emission spectrum off circumstellar dust.

Key words: techniques: polarimetric – circumstellar matter – stars: formation – stars: individual: Herbig Ae/Be – stars: pre-main-sequence.

1 INTRODUCTION

Despite the important role of massive stars in the evolution of the interstellar medium and unlike their counterpart low mass stars that are thought to be formed via magnetospheric accretion (Muzerolle et al. 1998), their accretion mechanism is still open to debate. Observationally, the detection of massive stars is challenging as they reside far away and are deeply embedded in their natal clouds. As an alternative to massive stars, the intermediate mass Herbig Ae/Be (HAeBe) stars are the best candidates to address this issue. They are optically visible and bridge the gap between low and high mass stars. They were first identified by Herbig as having a spectral type A or B with emission lines (Herbig 1960). The current view is that HAeBe stars are surrounded

by disks through which material continues to accrete onto the star (e.g. Ilee et al. 2014), although the precise scenario is not known (for reviews on the topic, see Grady et al. 2015; Kraus 2015; Beltrán & de Wit 2016).

In order to make progress, one needs to study the circumstellar environment through which the material accumulates onto the star via accretion channels. This requires methods capable of probing the matter very close to the star, as this is where the accretion action happens. A key point is the observation whether the ionised region around the star is spherically symmetric at small scales or not. If it is not, then the possibility that a flattened structure is observed lends support to the disk accretion scenario responsible for the formation of such stars. Studying the circumstellar environment at these small scales is possible through linear spectropolarimetry, measuring the scattering of photons off free electrons in a dense, ionised gas.

The idea of spectropolarimetry is that in the ionised region, free electrons scatter and polarise continuum photons from the central star. If the geometry is not circu-

^{*} Based on observations collected at the European Southern Observatory (ESO), Paranal, Chile under programme 088.C-0858(A), 088.C-0858(B) and 088.C-0858(C).

[†] E-mail: pykma@leeds.ac.uk

Table 1. HAEBe Observations. The V magnitude and spectral type are listed in column 3 & 4. The spectral type is taken from Ababakr et al. (2015) and Fairlamb et al. (2015) while the V magnitude is taken from Vieira et al. (2003) and SIMBAD. The integration times (column 8, 9 & 10) denote the total exposures in V (4560 - 5860 Å), R (5750 - 7310 Å) and Z (7730 - 9480 Å) bands.

Name	Other name	V	Spec. type	Date			V	Exposure (s)	
				V	R	Z		R	Z
PDS 27	DW CMa	13.0	B3	04-02-12	04-02-12	04-02-12	8×340	24×50	16×120
PDS 37	Hen 3-373	13.5	B3	05-02-12	05-02-12	05-02-12	16×340	24×70	16×100
CPD-485215	Hen 3-847	10.6	B6	20-01-12	10-03-12	03-03-12	8×150	32×15	16×90
R Mon	MWC 151	11.8	B8	19-02-12	01-02-12	01-02-12	4×340	12×85	12×80
V380 Ori		10.7	A0	03-01-12	12-10-11			12×85	
					03-01-12	10-11-11	8×60	16×20	12×20
					12-10-11			12×20	
PDS 133	SPH 6	13.1	B6		21-01-12	21-01-12		16×150	8×340
BF Ori		9.7	A2		12-10-11	12-11-11		8×75	8×90
MWC 275	HD 163296	6.9	A1		01-04-12	30-03-12		32×2.5	16×7.5
GU CMa	HD 52721	6.6	B1		07-01-12	07-01-12		24×2	24×5
HD 104237	PDS 61	6.6	A7		16-01-12	16-01-12		40×1	24×5
HD 85567		8.6	B7		30-12-11	08-12-11		8×5	16×30
HD 98922	Hen 3-644	6.8	A0	30-12-11	16-01-12			8×5	24×5
								40×1.5,16×1	

lar on the sky, for example in the case of flattened disk, a net polarisation can be detected. However, emission photons undergo less scattering as they emerge further away from the central star. If we are to measure the polarisation as a function of wavelength, this difference in scattering will be visible as a change in polarisation across the line, which is often simply referred to as the “line effect”. The observed de-polarisation across the $H\alpha$ line constituted the first evidence that the class of Be stars were surrounded by disks (Clarke & McLean 1974; Poeckert & Marlborough 1976). This was only much later confirmed by direct observations (e.g. Quirrenbach et al. 1994 based on image reconstruction of interferometric data; Wheelwright et al. 2012 using sub-milliarcsecond precision spectro-astrometry).

Oudmaijer & Drew (1999), Vink et al. (2002) and Mottram et al. (2007) extended the use of the technique to HAEBe objects. Vink et al. (2002) found that 7 out of 12 Herbig Be (HBe) objects they observed have a depolarisation line effect across $H\alpha$, very similar to what was found in Be stars. As the line-effect becomes less pronounced for lower inclinations, and would disappear for a face-on disk, which is circular on the sky, the detection statistic strongly suggests that all HBe stars are surrounded by small disks with sizes of order several stellar radii. In contrast, they found a different line effect for Herbig Ae (HAe) objects, where enhanced *polarisation* across the $H\alpha$ was found in 9 out of 11 stars. They proposed that the line itself is intrinsically polarised since part of the emission lines originate from a compact region, where the accretion takes place. Vink et al. (2005) found that HAe stars have a similar spectropolarimetric signature as the lower mass T Tauri stars with HBe stars having a different signature.

McLean (1979) reported a different line effect, across the absorption component of the emission line which is often called the McLean effect. The general idea is that the absorption blocks the unscattered light from the beam, and photons originally emitted in different directions are scattered into the line of sight, resulting in enhanced polarisa-

tion across the absorption. An alternate hypothesis was provided by Kuhn et al. (2007), who proposed the polarisation can be caused by selective absorption due to optical pumping of an anisotropic radiation field. In addition, Kuhn et al. (2011) point out that resonant line scattering, which potentially also produces line polarisation, predicts that the lines within the Ca II near-infrared triplet around 8500 Å will be differently polarised from each other. For a recent review on the use of linear spectropolarimetry, see Vink (2015).

In this work we aim to expand the existing spectropolarimetric work that was mostly aimed at $H\alpha$ by observing other emission lines probing different volumes and conditions than $H\alpha$. Here we present a spectropolarimetric study of a sample of 12 HAEBe objects. The new feature of the current study is the broad wavelength range from 4560 Å to 9480 Å, covering almost the entire optical spectrum. The paper is organised as follows. In Section 2 we discuss the sample selection criteria, the details of the observations and data reduction. In Section 3 we present the results starting with continuum polarisation and then discussing line spectropolarimetry. The analysis is provided in Section 4. We conclude in Section 5.

2 OBSERVATIONS

2.1 Source selection

Twelve objects were selected for this work from the X-shooter project of 91 HAEBe stars (Oudmaijer et al. 2011; Fairlamb et al. 2015). The main reason for choosing these, was the presence of strong emission lines which allows for a good determination of their spectropolarimetric properties. The targets were originally selected from the HAEBe catalogue of The et al. (1994) and candidates of Vieira et al. (2003). They are presented in Table 1, alongside their spectral type and V magnitudes. The spectral type is taken from Ababakr et al. (2015) and Fairlamb et al. (2015) while the V magnitude is taken from Vieira et al. (2003) and SIMBAD.

The results of PDS 27 and PDS 37 have been published elsewhere in a study dedicated to these two objects, but we keep them in here (Ababakr et al. 2015).

2.2 Spectropolarimetric observations

The spectropolarimetric data were obtained with the FORS2 spectrograph mounted on ESO's VLT in Chile. The 1400V, 1200R and 1027Z gratings centred at 5200 Å, 6500 Å and 8600 Å respectively were used with a 4096×2048 pixel CCD to cover the entire optical range from 4560 Å to 9480 Å. A spectral resolution of $R = 3800, 4800, 4800$ was achieved in the *V*, *R*, and *Z* bands respectively, using the 0.5 arcsec slit. The dates and the exposure times for each band are given in Table 1.

The optical polarimeter in FORS2 was employed for the linear polarisation observations. It consists of a rotating half-wave plate and a calcite block. The half-wave plate can be set to various angles to get *QU* Stokes parameters while the calcite block separates the light into two perpendicularly polarised light beams, the ordinary (O) and extraordinary (E) beam. Four exposures with the half-wave plate set at angles $0^\circ, 45^\circ, 22.5^\circ$, and 67.5° provide a complete set of observations. At each angle, four spectra are obtained; the O and E beam of the object and sky respectively. Several cycles of observation at the above 4 angles were taken for each object to check for the consistency of the polarisation and its features. Several polarised standard stars and unpolarised standard stars were observed to calibrate the instrumental polarisation and angle offset.

Spectropolarimetry is a photon-hungry method. Typical line effects are of order 0.5% and to properly sample the polarisation behaviour as a function of wavelength, a polarisation precision of order 0.1% per pixel is therefore required. This corresponds to signal-to-noise ratios of order 1000. We used long exposure times for faint objects and several short exposure times for objects with strong $H\alpha$ lines in order to avoid saturation of the CCD.

2.3 Data reduction

The data reduction was carried out using GASGANO and FORS pipeline v4.9.18, which includes bias subtraction, flat fielding, sky subtraction, extraction and wavelength calibration of the O and E spectra. The Stokes parameters were determined from the O and E spectra. Finally, the percentage of linear polarisation, *P*, and polarisation angle, θ , were obtained according to the following equations:

$$P = \sqrt{Q^2 + U^2} \quad (1)$$

$$\theta = \frac{1}{2} \arctan \left(\frac{U}{Q} \right) \quad (2)$$

For the analysis purposes, the data were imported into the IRAF (Tody 1993) and POLMAP package (Harries 1996) maintained by Starlink. The individual data sets were combined to improve the quality of the data. Four polarised and three zero polarised standard stars were selected from the sample of Fossati et al. (2007) for polarimetric calibrations. The instrumental polarisation is found to be $\sim 0.16\%$, from the observation of unpolarised standard stars. The angle offset is found to be 0.5° from the observation of polarised

standard stars. In order to clearly visualise the line effect, the change in polarisation across the lines, we rebin the polarisation spectra to a maximum polarisation error per bin. We performed the rebinning of the spectra very carefully to avoid losing the line effect signature. We did not correct the data for the instrumental and interstellar polarisation. These two parameters only add a, small, wavelength independent vector to the observed *Q* and *U* parameters whereas our main aim in this work is the detection of polarimetric change across the lines. However, as the polarisation is a vector quantity, the interstellar polarisation could change the appearance of the polarisation signature across the line (see e.g. Oudmaier et al. 1998 in HD 87643). Therefore, careful analysis is needed to characterise the line effect.

2.4 The Optical Spectrum

In the optical range from 4560 Å to 9480 Å, the spectra show numerous spectral lines in emission and absorption. The entire spectrum of PDS 27 is presented in Fig. 1 to show the range of the observed spectra and the identified spectral lines.

The $H\alpha$ lines are the strongest with line peak to continuum ratios ranging from ~ 2 to ~ 20 . In all targets, $H\alpha$ is in emission, as shown in Fig. 2. The $H\alpha$ lines exhibit various different profiles. These include pure emission lines, double peaked emission with central absorption through to P Cygni profiles. GU CMa, CPD-485215 and V380 Ori display a pure emission line, R Mon and BF Ori show a double peaked emission line with central absorption. The remaining seven objects display P Cygni profiles, for two of which we also have $H\beta$ data. For both spectra that contain $H\beta$, the absorption component in $H\beta$ is deeper than in $H\alpha$. In addition to Balmer series, weak Paschen lines are also seen in emission for most objects.

The Ca II triplet lines at 8498, 8542 and 8662 Å are observed in all objects apart from GU CMa and CPD-485215. They are all in emission apart from BF Ori where they are in absorption. The line to continuum ratio is in the range 1.5 to 10.5. The Ca II doublet at 8912 and 8927 Å is present in all objects apart from GU CMa, MWC 275 and CPD-485215. The lines are in emission in all objects apart from HD 104237 and BF Ori where the lines are in absorption.

Three He I lines at 5876, 6678 and 7065 Å are observed in all objects. The lines are in absorption in six objects including PDS 27, PDS 37, R Mon, HD 85567, GU CMa and BF Ori. PDS 133, HD 104237, V380 Ori and HD 98922 have the lines in emission. Inverse P Cygni profiles, weak emission and strong absorption He I lines are detected in the spectra of MWC 275 and CPD-485215 and indicate infalling material.

Several forbidden [Fe II] at 4814, 5158, 5262, 5333, 7155 and 8616 Å lines are observed in the spectra of R Mon and CPD-485215. [S II] at 6716 and 6730 Å is also seen in the spectra of R Mon. In addition, strong [O I] at 6300, 6364 Å is present in the spectra of R Mon, CPD-485215 and PDS 133. However, [O I] lines are either absent or very weak in the spectra of the remainder of the targets. Unlike the cases of R Mon and CPD-485215, the [O I] lines in the spectra of PDS 133 are broad and double peaked which may suggest that the forbidden lines emerge from a rotating disk. This has been suggested before for H AeBe stars (Acke et al. 2005),

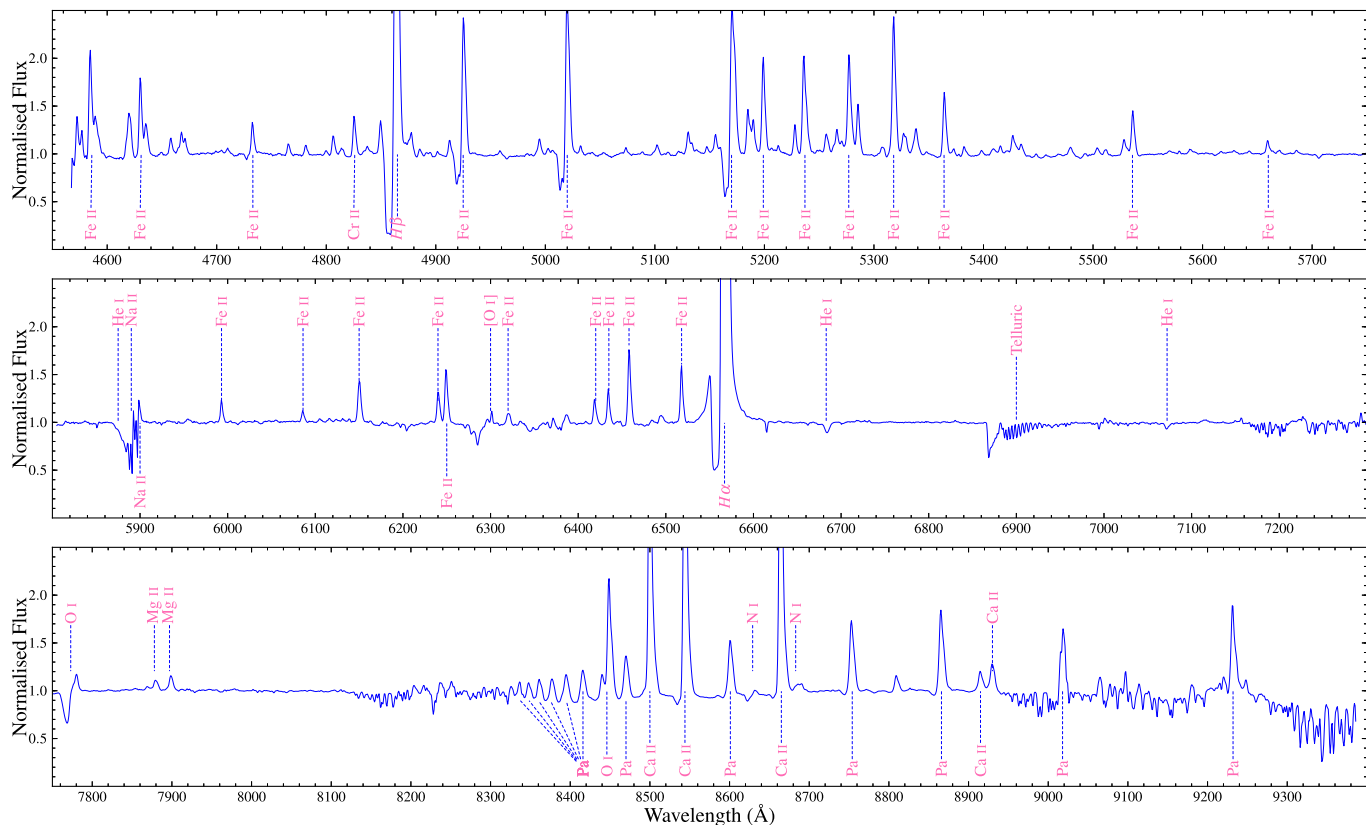


Figure 1. Normalised flux versus wavelength (\AA) spectra of PDS 27 in the range from 4560 \AA to 9480 \AA , the observed spectral lines are identified.

although the broad line could also indicate a disk-wind (see e.g. Ignace & Brimeyer 2006).

In summary, we observe many strong emission lines which allows us to investigate spectropolarimetric line effects which had never been done before studied for most of these lines.

3 RESULTS

3.1 Continuum Polarisation

The continuum polarisation is measured for the entire spectrum and the results for the polarimetric standard stars are shown in Fig. 3, while those for the H AeBe stars are plotted in Fig. 4. The data are rebinned using a coarse sampling of ~ 250 Å per bin, to minimise errors.

Typically, the observed continuum polarisation is a vector addition of the interstellar polarisation and the intrinsic polarisation which is due to scattering of star light by circumstellar dust and free electrons. The interstellar polarisation is caused by dichroic absorption of aligned dust grains. Its wavelength dependence is well understood and explained by Serkowski et al. (1975). They found that the linear polarisation follows an empirical curve according to the following equation:

$$\frac{P(\lambda)}{P_{max}} = \exp \left[-k \ln^2 \left(\frac{\lambda_{max}}{\lambda} \right) \right] \quad (3)$$

where λ_{max} is the wavelength where the polarisation is at its

maximum value, P_{max} , and k is the width of the empirical curve. Typically, the polarisation peaks in the visual band at ~ 5500 Å, but can be in the range of 4500-8000 Å. k was initially taken to be a constant value of $k = 1.15$. However, it has been found that the value of k depends on the value of λ_{max} , and is sensitive to the size distribution of the dust particles (Whittet et al. 1992). In order to assess whether the observed polarisation may have an interstellar dust component, we fit the Serkowski law (Equation 3) to our targets and polarised standard stars. λ_{max} , P_{max} and k are taken as a free parameters. The Serkowski law provides - as expected - an excellent fit to the polarised standard stars as shown in Fig. 3. The figure also shows that the polarisation angle remains constant over different bands.

The best fit to our targets is provided in Fig. 4. The stars generally follow the Serkowski law but not as well as the standard stars. In some objects, the polarisation spectra peak at much longer wavelengths than the V band while, in addition, the polarisation angle changes over different bands in all objects. This overall behaviour would suggest that a fraction of the observed polarisation is due to interstellar dust, but that an intrinsic contribution is present. This is also consistent with the polarisation angle. For all objects, the observed polarisation angle changes over different bands, indicating the presence of intrinsic polarisation. The deviation of the angle ranges from 1° to 30° (see Fig.4). The polarised standards did not show a significant deviation in the observed polarisation angles.

We note that the continuum polarisation and the po-

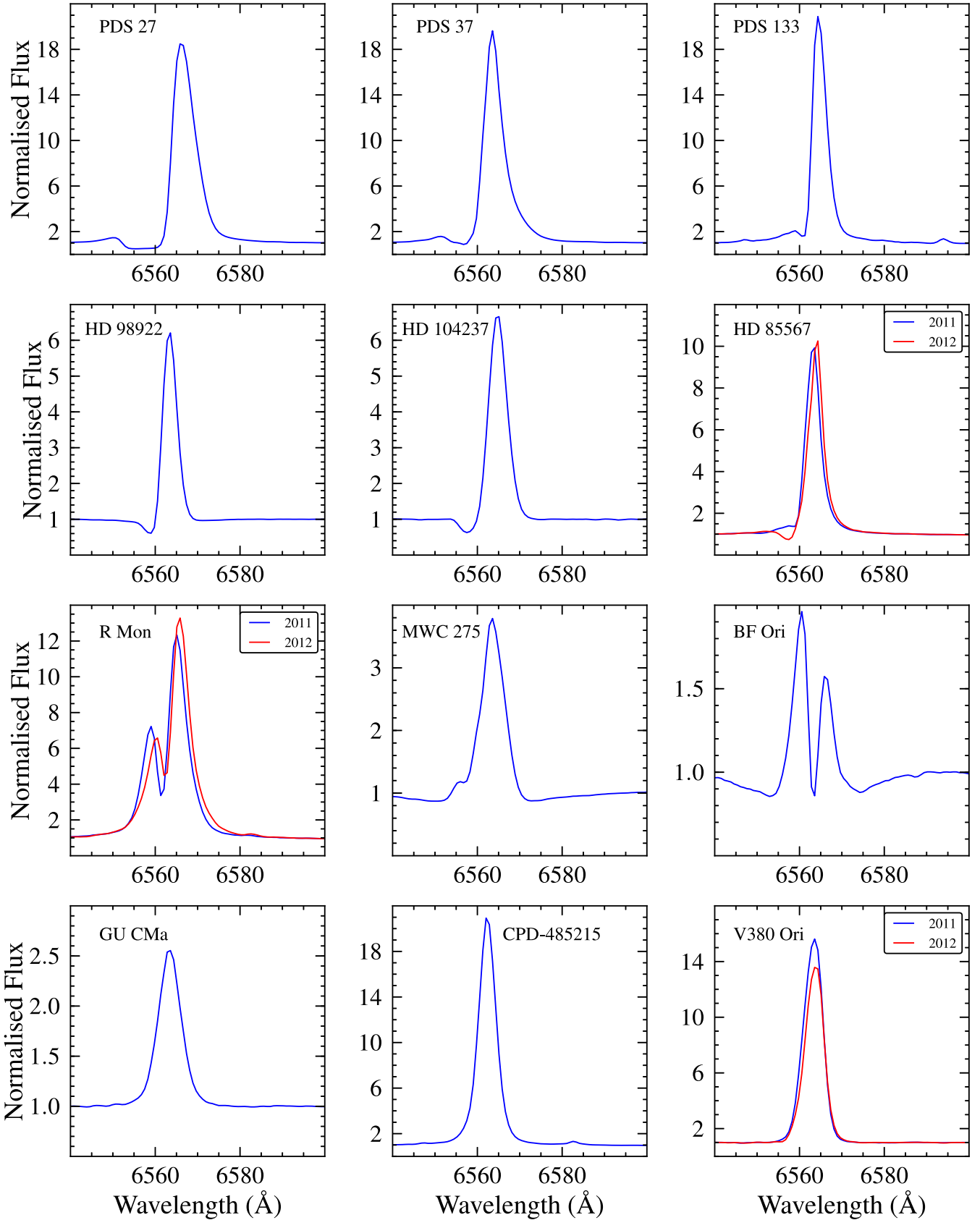


Figure 2. The H α line profiles, the spectra are normalised to one. The spectra of HD 85567, R Mon and V380 Ori are presented for two observation epochs: 2011 (blue solid line) and 2012 (blue solid line).

Table 2. The continuum polarisation of the targets measured in the following wavelength regions: *B* band centred at 4700 Å; *V* band centred at 5500 Å; *R* band centred at 7000 Å; *I* band centred at 9000 Å. The polarisation was measured over a wavelength range of 250 Å either side of the central wavelength, except for the *B* band where it was 125 Å either side. All the errors are differential, where the instrumental error is $\sim 0.16\%$ in polarisation and $\sim 0.5^\circ$ in angle (see text in Section 2.3 for details).

Object	<i>B</i>		<i>V</i>		<i>R</i>		<i>I</i>	
	$P_{cont}(\%)$	θ_{cont}°	$P_{cont}(\%)$	θ_{cont}°	$P_{cont}(\%)$	θ_{cont}°	$P_{cont}(\%)$	θ_{cont}°
PDS 27	8.60 ± 0.03	18.60 ± 0.10	9.00 ± 0.01	18.90 ± 0.01	8.80 ± 0.01	18.40 ± 0.04	7.50 ± 0.01	18.10 ± 0.03
PDS 37	4.70 ± 0.04	130.00 ± 0.30	5.10 ± 0.01	130.80 ± 0.01	5.20 ± 0.01	130.00 ± 0.06	4.40 ± 0.01	133.40 ± 0.05
CPD-485215	1.25 ± 0.01	19.30 ± 0.30	1.30 ± 0.01	15.30 ± 0.06	1.70 ± 0.01	9.50 ± 0.20	1.90 ± 0.01	6.70 ± 0.20
R Mon	11.20 ± 0.04	80.60 ± 0.10	11.20 ± 0.02	80.00 ± 0.05	12.15 ± 0.01	67.70 ± 0.04	12.10 ± 0.01	60.15 ± 0.03
V380 Ori	0.60 ± 0.01	90.80 ± 0.70	0.70 ± 0.01	93.20 ± 0.30	8.10 ± 0.02	69.40 ± 0.07	0.10 ± 0.01	124.00 ± 3.00
V380 Ori					0.70 ± 0.01	98.40 ± 0.06		
PDS 133					0.70 ± 0.02	95.15 ± 1.00		
BF Ori					2.30 ± 0.04	37.70 ± 0.50	2.10 ± 0.03	38.30 ± 0.05
MWC 275					0.70 ± 0.01	1.60 ± 0.20	0.67 ± 0.01	14.84 ± 0.28
GU CMa					1.60 ± 0.01	14.60 ± 0.01	1.40 ± 0.01	14.45 ± 0.09
HD 104237					0.35 ± 0.01	174.60 ± 0.60	0.58 ± 0.01	182.89 ± 0.35
HD 85567					0.38 ± 0.01	133.90 ± 0.60	0.23 ± 0.01	154.02 ± 0.61
					0.26 ± 0.02	134.50 ± 2.10		
HD 98922					0.40 ± 0.01	174.90 ± 0.30	0.58 ± 0.01	177.90 ± 0.30

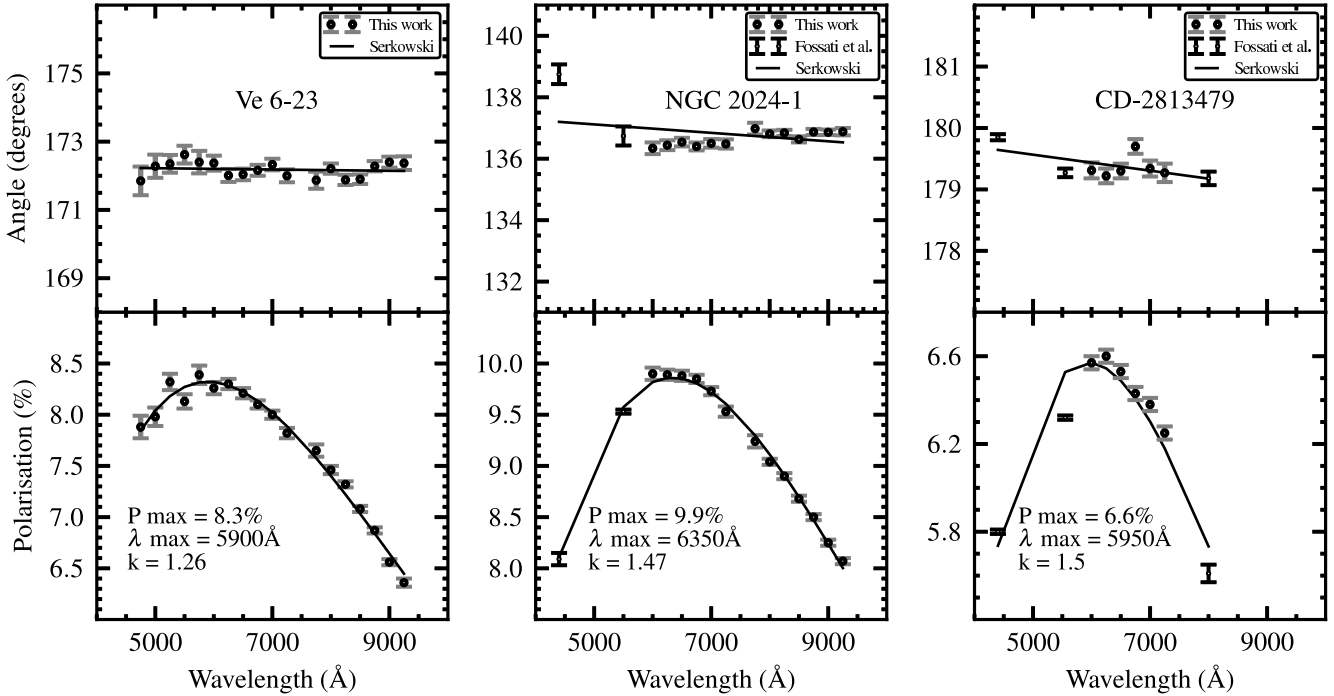


Figure 3. The polarisation and polarisation angles as a function of wavelength for the polarised standard stars. The data for this work are presented in black solid circles and were coarsely sampled to improve the error bars. The data in *B* and *V* for NGC 2024-1, and in *B*, *V* and *I* (black dots) are taken from Fossati et al. (2007). The black lines denote the best-fitting Serkowski law to the data.

larisation angle jump from one setting to another for some objects (see Fig.4). This is particularly striking in PDS 37, R Mon and MWC 275. This might be because the objects are extended, and that a slightly different positioning of the slit could result in slightly different polarisation to be measured, which we shall discuss later.

To facilitate comparison with past and future observations, we measured the continuum polarisation at the *B*, *V*,

R and *I* bands and the results are summarised in Table 2. The linear continuum polarisation ranges from $\sim 0.3\%$ in the very low polarised star HD 85567 to $\sim 12\%$ in the highly polarised star R Mon. The data of two epochs are provided for three objects, R Mon, V380 Ori and HD 85567. R Mon shows a strong variability of order of $\sim 4\%$ in the *R* band between these two epochs. V380 Ori shows similar polarisation values and HD 85567 shows a little variation. The

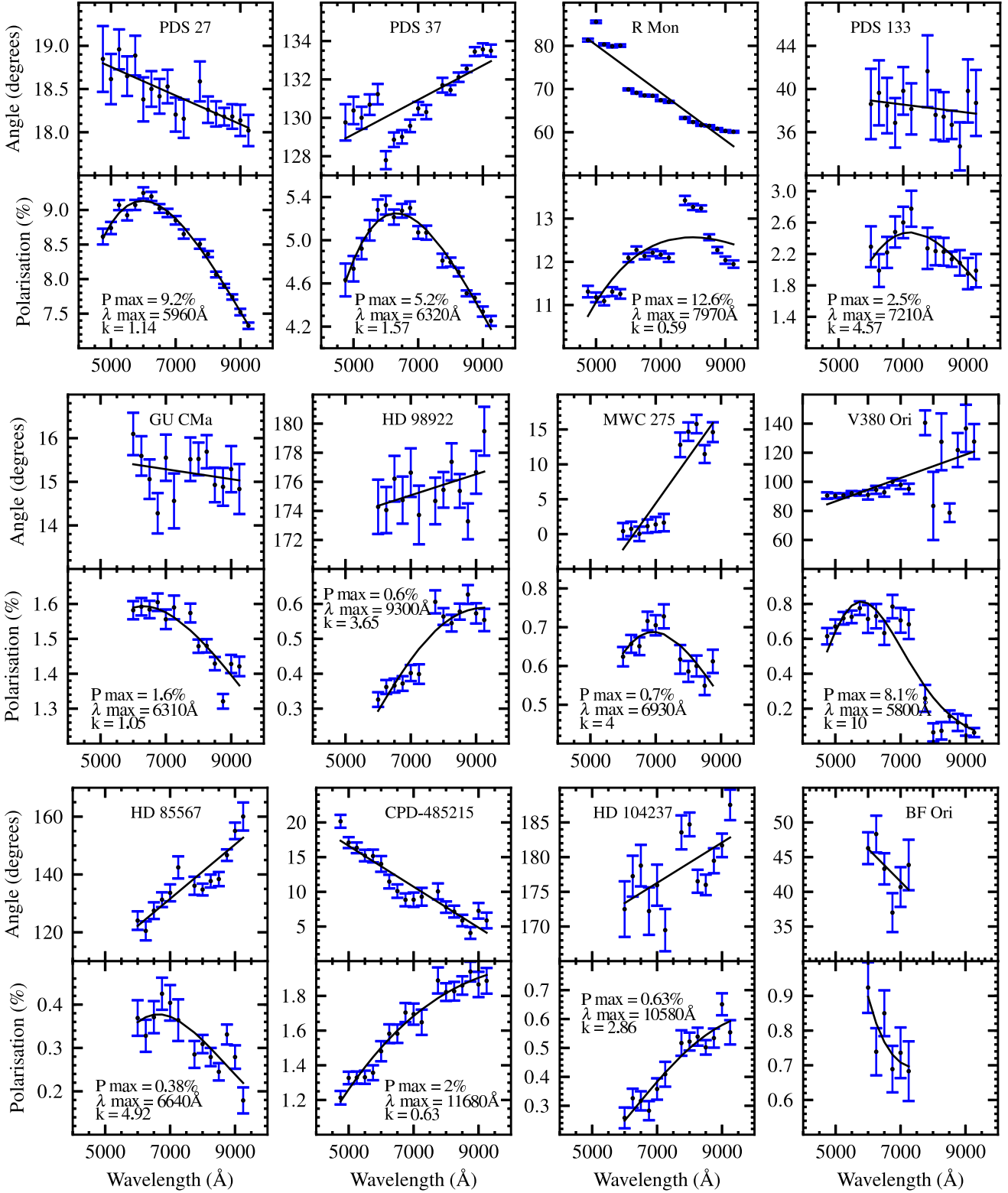


Figure 4. As the previous figure, but now for the HAeBe stars. The polarisation is shown in the lower panel while the polarisation angle is shown in the upper panel. The black lines denote the best fitting Serkowski law to the data.

Table 3. Previous measured continuum polarisation. Column 2 gives the band at which the polarisation was measured. Columns 3 and 4 list the measured polarisation percentage and polarisation angle. The references are presented in the last column.

Object	Band	$P_{cont}(\%)$	θ_{cont}°	Ref.
PDS 37	<i>V</i>	3.253 ± 0.104	120.1 ± 1.0	1
CPD-485215	<i>V</i>	0.348 ± 0.035	20.7 ± 3.0	1
R Mon	<i>V</i>	12.0 ± 1.2	91 ± 3	2
	<i>U</i>	11.1 ± 0.7	85.7 ± 1.8	3
	<i>B</i>	11.1 ± 0.4	86.6 ± 1.1	3
	<i>V</i>	12.3 ± 0.5	89.4 ± 1.2	3
	<i>R</i>	12.6 ± 0.3	83.5 ± 0.8	3
	<i>I</i>	12.1 ± 0.4	94.5 ± 0.9	3
V380 Ori	<i>V</i>	0.98 ± 0.10	86 ± 3	2
	<i>R</i>	1.26 ± 0.01	96 ± 1	4
	<i>U</i>	0.08 ± 0.16	151 ± 57	3
	<i>B</i>	0.80 ± 0.06	88.8 ± 2.1	3
	<i>V</i>	0.98 ± 0.06	86.2 ± 1.8	3
	<i>R</i>	1.31 ± 0.14	74.4 ± 3.2	3
BF Ori	<i>I</i>	1.25 ± 0.18	84.9 ± 4.2	3
	<i>R</i>	0.6 ± 0.1	58 ± 1	5
	<i>R</i>	0.886 ± 0.017	52.0 ± 0.6	6
	<i>V</i>	0.46 ± 0.01		7
GU CMa	<i>R</i>	1.15 ± 0.01	19 ± 1	4
	<i>R</i>	0.8 ± 0.1	24 ± 1	5
	<i>R</i>	1.726 ± 0.006	27.0 ± 0.1	6
HD 104237	<i>V</i>	0.032 ± 0.063	167.2 ± 56.5	1
HD 85567	<i>V</i>	0.478 ± 0.035	105.7 ± 2.0	1
HD 98922	<i>U</i>	0.515 ± 0.087	152.8 ± 5.0	8
	<i>B</i>	0.201 ± 0.070	168.4 ± 14.1	8
	<i>V</i>	0.235 ± 0.051	160.5 ± 6.0	8
MWC 275	<i>V</i>	0.417 ± 0.035	36.0 ± 2.5	1
	<i>V</i>	0.225 ± 0.012	29.8 ± 1.6	8
	<i>R</i>	0.284 ± 0.014	35.5 ± 1.5	8
	<i>I</i>	0.351 ± 0.018	38.3 ± 1.5	8
	<i>V</i>	0.02 ± 0.01		7

References. 1:Rodrigues et al. (2009), the errors on the polarisation angle for this reference are calculated from $0.5 \times \arctan(\sigma_P/P)$; 2:Hillenbrand et al. (1992); 3:Vrba et al. (1979); 4:Oudmaijer & Drew (1999); 5:Wheelwright et al. (2011); 6:Vink et al. (2005); 7:Oudmaijer et al. (2001); 8:Yudin & Evans (1998), we calculated the average values for MWC 275, taken on the same day.

literature values for the objects are summarised in Table 3. The polarised standard stars are consistent with the literature values. The HAeBe stars are broadly consistent with the previous measurements, but there is some variation in the polarisation data.

The polarisation variability in the degree of polarisation and/or polarisation angle is a common phenomenon among HAeBe objects (Grinin 1994; Jain & Bhatt 1995). Its origin is thought to be caused by the intrinsic polarisation over time as the interstellar polarisation is unlikely to be variable over a short period of time.

3.2 Line spectropolarimetry

Most of the previous spectropolarimetric studies have been performed on the strong $H\alpha$ emission lines. However, the advantage of this study is that the long spectral coverage allows us to perform linear spectropolarimetry on lines that had never been studied in this manner before. We begin by

discussing the results of the strongest hydrogen recombination lines before we discuss other lines.

3.2.1 Hydrogen recombination lines

Spectropolarimetry was performed on all hydrogen lines including $H\alpha$, $H\beta$ and the Paschen lines. The spectropolarimetric data around $H\alpha$ are shown in a so-called “triplet” in the upper half of Fig. 5. In this triplet, the Stokes I (normal intensity) is shown in the lower panel, the polarisation percentage in the middle, while the position angle (PA) is shown in the upper panel. The results are also represented in a Stokes (Q , U) diagram (bottom) in Fig. 5 using the same wavelength range of the triplet spectra, but sometimes with a different binning. Ten out of the twelve objects display a clear line effect across $H\alpha$ while the remaining two, BF Ori and HD 104237, show a potential line effect. The observed line effects across $H\alpha$ are of order of $\sim 0.2\%$ to $\sim 7\%$ in the case of R Mon. The change in polarisation occurs across the emission lines, the absorption components or the entire line profiles.

The spectropolarimetric properties of $H\alpha$ for each target are listed in Table 4. Columns 3, 4 & 5 list the spectroscopic characterisation of Stokes I, the intensity spectrum. Generally, the lines are stronger in HBe objects than in H Ae objects. The final three columns represent the line polarimetric properties, i.e. the depolarisation, line polarisation and McLean effects as introduced in Sec. 1.

The intrinsic polarisation angle is measured from the slope of the loop of the line in the (Q , U) diagram following Wheelwright et al. (2011). From the analysis of the (Q , U) diagram, we can determine the direction of intrinsic polarisation on the sky. We have measured the intrinsic polarisation from the slope of the loop across the line in the (Q , U) diagram of Fig. 5. This gives two different results depending on the type of the line effect. In the case of line depolarisation, the intrinsic angle is measured from the line to continuum while for line polarisation it is measured from continuum to the line resulting in a 90° difference from the former. This 90° difference in polarisation is equivalent to 180° on the sky, for that reason the direction of the vector in the (Q , U) diagram is crucial, and this depends on the type of polarisation we observe. For the objects displaying the McLean effect, the angle is measured from the continuum to the line.

The data for the next strongest hydrogen recombination line, $H\beta$, is available for five objects. Two of these, R Mon and CPD-485215, show a clear change in polarisation across this line and the results are presented in Fig. 6. The Paschen lines are much weaker than the Balmer series and only R Mon shows a line effect across these lines.

3.2.2 Ca II lines

The Ca II triplet at 8498, 8542 and 8662 Å originates at larger distances from the central star than $H\alpha$ because of its lower ionisation energy. Only two objects out of twelve, show a change in polarisation across these lines. MWC 275, as shown in Fig. 7, displays a clear change across these lines. The change is as broad as the emission lines and is clear in both polarisation and polarisation angle. R Mon also shows a change in polarisation across these lines (see Fig. A1) in

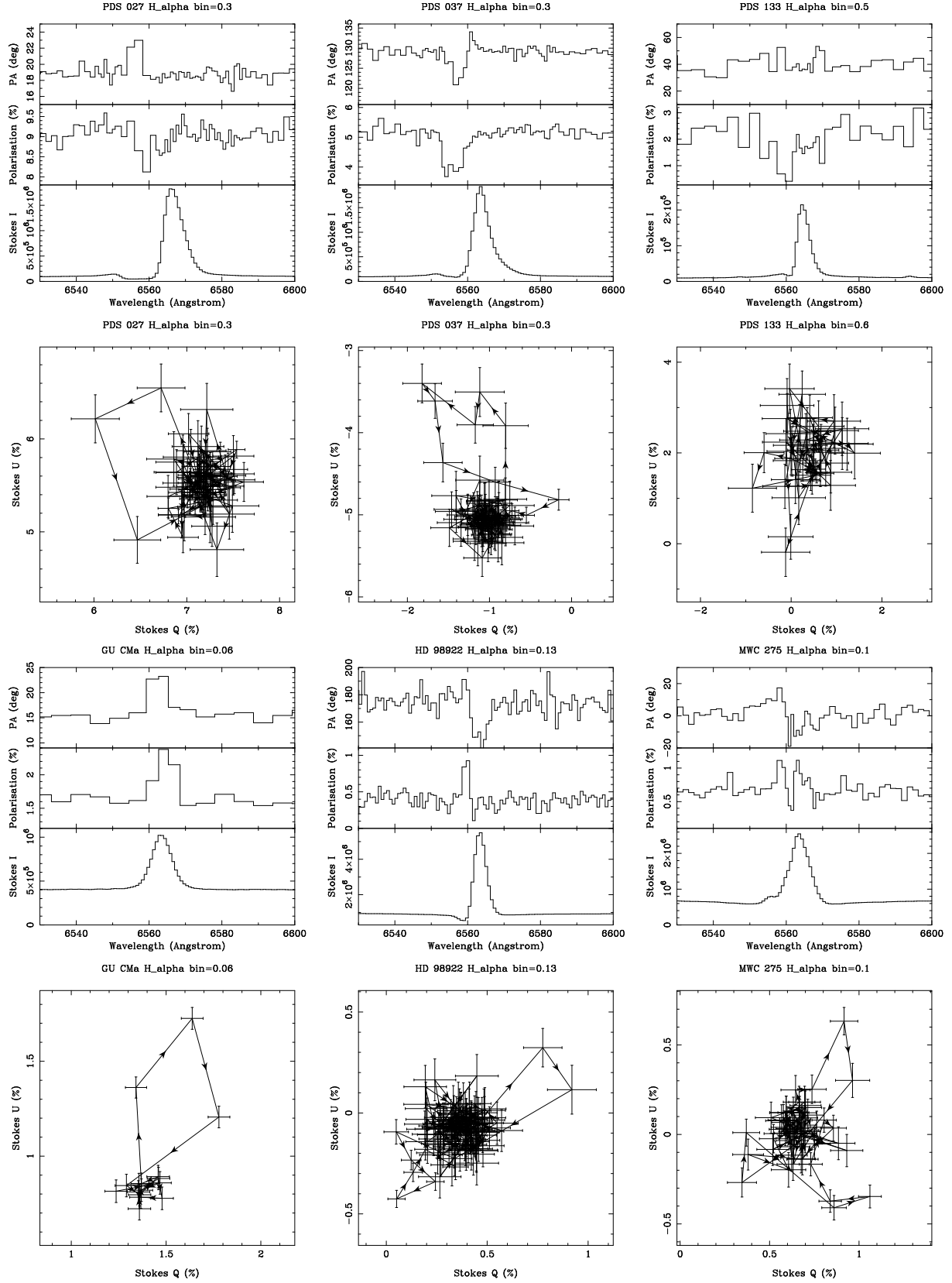


Figure 5. H α spectropolarimetry of the stars. The data are presented as a combination of triplots (top) and (Q, U) diagrams (bottom). In the triplot polarisation spectra, the Stokes intensity (I) is shown in the bottom panel, polarisation (%) in the centre, while the position angle (PA) is shown in the upper panel. The Q and U Stokes parameters are plotted against each other below each triplot. The data are rebinned to a constant error in polarisation, which is indicated at the top of each plot. The arrows in the (Q, U) diagrams indicate the polarisation moves in and out of the line effect from blue to red wavelengths.

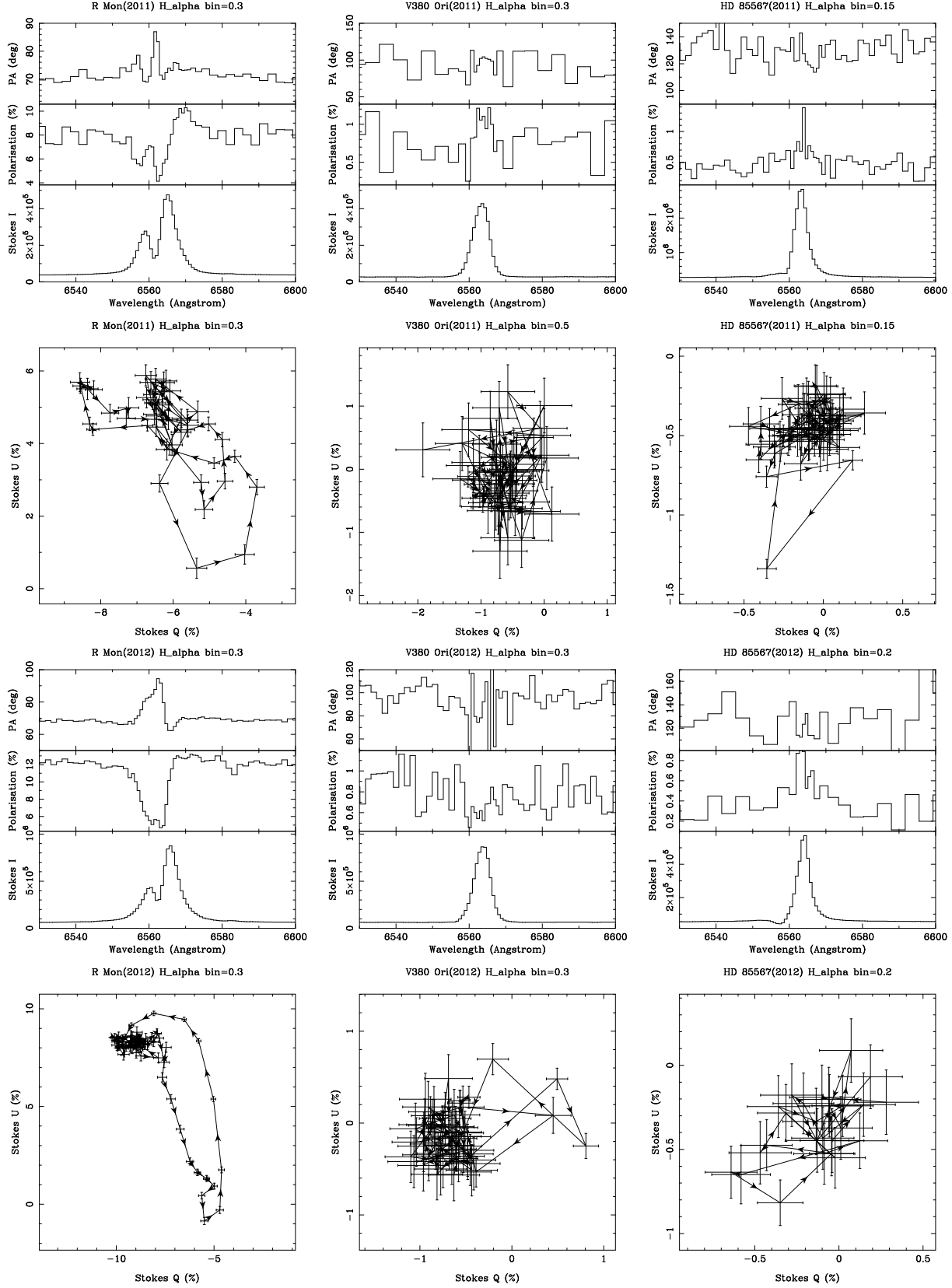


Figure 5. continued

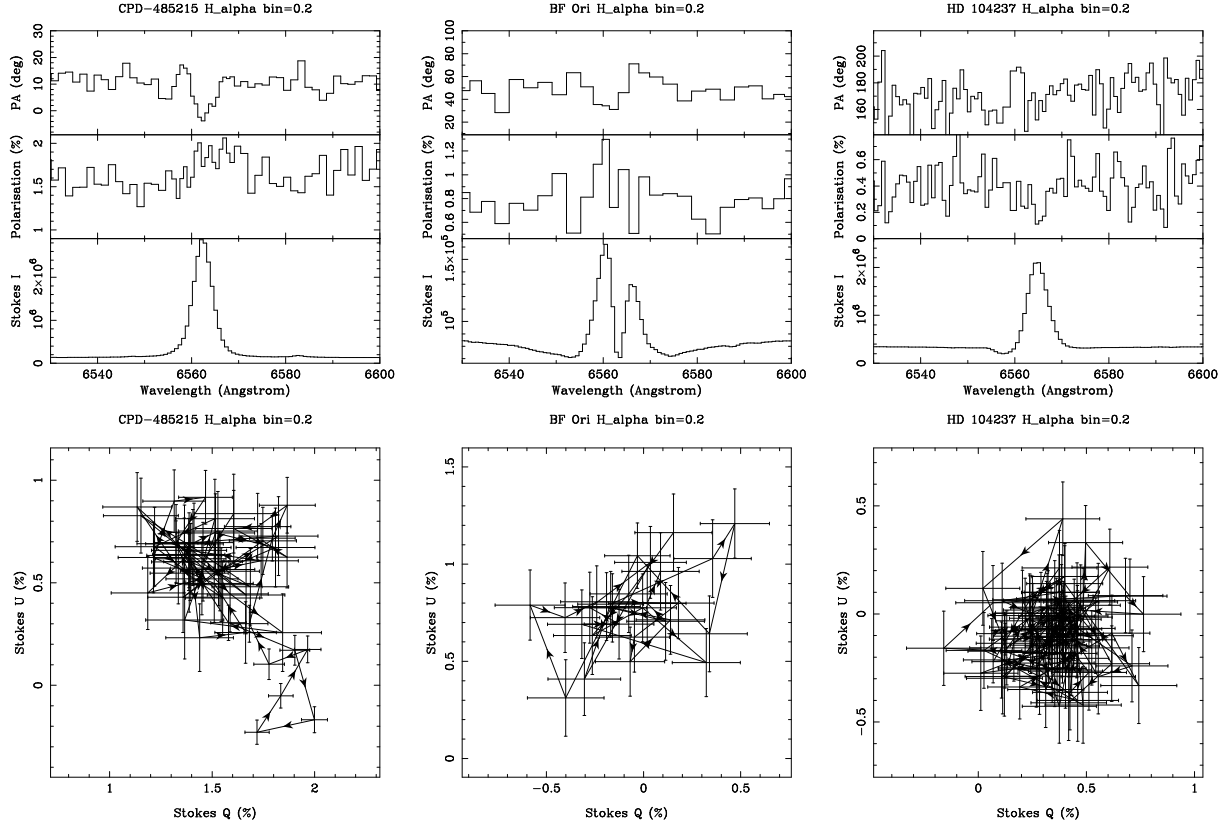


Figure 5. continued

Table 4. The H α line results: columns (3), (4) and (5) list the Stokes (I) characteristics; columns (6), (7) and (8) list line spectropolarimetry characteristics of each target. Column (8) provides an estimation of the intrinsic polarisation PA derived from line excursions in the (Q , U) diagram (see text for details). Errors in the EW measurements are typically 5%, the uncertainty in intrinsic polarisation angle is approximately 10° .

Object	Spec. type	line profile	EW (\AA)	Line/cont.	Line effect	Classification	θ_{intr}°
PDS 27	B3	P Cygni	-120.8	18.0	Yes	McLean	77
PDS 37	B3	P Cygni	-122.6	19.4	Yes	McLean	56
PDS 133	B6	P Cygni	-94.5	20.7	Yes	McLean	126
HD 98922	A0	P Cygni	-17.9	6.0	Yes	McLean\Depol.	22
R Mon(2011)	B8	Double-peaked	-98.6	12.6	Yes	Depol.	63
R Mon(2012)		Double-peaked	-105.5	12.9	Yes	Depol.	57
GU CMa	B1	Pure emission	-11.1	2.6	Yes	Depol.	127
CPD-485215	B6	Pure emission	-100.8	19.6	Yes	Depol.	62
MWC 275	A1	P Cygni	-14.9	3.8	Yes	\sim Pol.	112
HD 85567(2011)	B7	P Cygni	-43.5	9.9	Yes	\sim Depol.	31
HD 85567(2012)		P Cygni	-42.1	10.2	Yes	\sim Depol.	22
V380 Ori(2011)	A0	Pure emission	-82.7	15.5	Possible		
V380 Ori(2012)		Pure emission	-71.1	13.6	Yes	\sim pol.	10
HD 104237	A7	P Cygni	-27.2	6.5	Possible		
BF Ori	A2	Double-peaked	1.0	1.9	Possible		

appendix A). PDS 37 shows a possible line effect in only the first two datasets while the second two datasets do not show such a line effect (Ababakr et al. 2015). Therefore, the line effect in PDS 37 is not a conclusive result based on the current data. The Ca II doublet at 8912 and 8927 \AA is also seen in the spectra of most objects. R Mon is the only object that shows a line effect across the Ca II doublet.

3.2.3 He I lines

The He I lines trace the very inner hot circumstellar environment as they have a very high excitation energy. Three He I lines at 5876, 6678 and 7065 \AA are seen in the spectra of all objects. These lines do not show any signs of a line effect. In most objects the lines are in absorption however, while those in emission are very weak, possibly too weak to show the line effect.

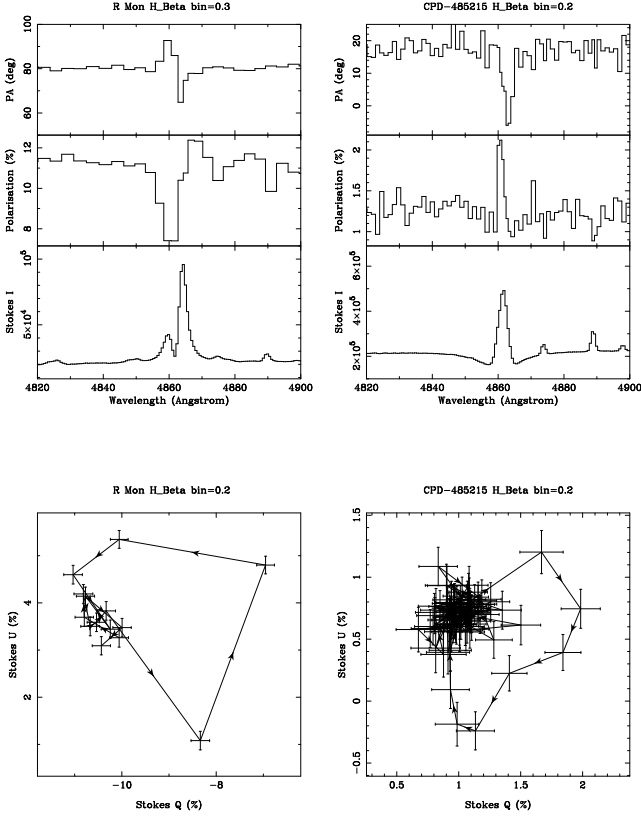


Figure 6. H β spectropolarimetry of R Mon and CPD-485215. See the caption of Fig. 5 for more details.

3.2.4 Forbidden lines

Most objects have forbidden emission lines, however line effects across them are limited to a few objects. All the [Fe II] lines show a depolarisation in R Mon and CPD-485215. Both [S II] display a clear depolarisation in the spectra of R Mon. [O I] lines also display a clear depolarisation in R Mon, CPD-485215 and PDS 133. However, the lines are broad and double peaked in PDS 133. The polarisation spectra of PDS 133 across [O I] at 6300 Å is presented in Fig. 8 and the remainder of the polarisation spectra of all forbidden lines are presented in Fig. A1.

3.2.5 O I and Fe II lines

Two O I lines at 7773 and 8446 Å are observable. R Mon and CPD-485215 show a clear change in polarisation across these lines. Several Fe II lines are observable in the spectra of all objects. However, only R Mon shows the line effect across these lines. The polarisation spectra can be seen in Fig. A1.

3.2.6 Summary on the occurrence of the line effect

We presented spectropolarimetry from 4560 Å to 9480 Å of a sample of H AeBe stars that were previously known to have a line effect across the H α line. We find that this phenomenon is very rare across lines other than H α . Strong emission lines such as H β and the Ca II near-infrared triplet are only seen with a line effect in just a few sources. We should perhaps

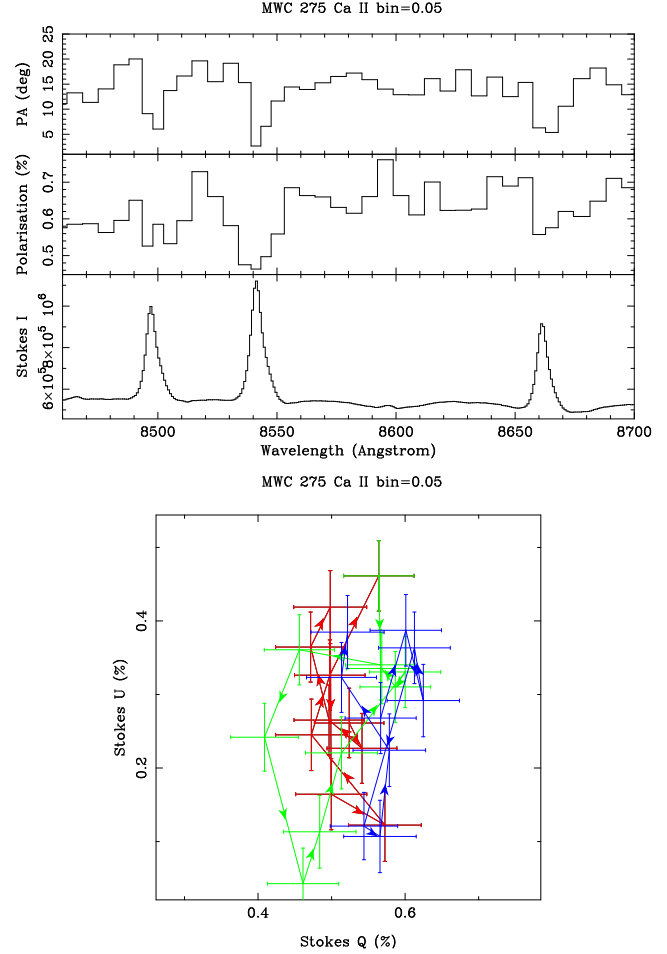


Figure 7. Ca II triplet polarisation data of MWC 275. In the (Q , U) diagram, the lines at 8498, 8542 and 8662 Å are plotted in red, green and blue solid lines. See the caption of Fig. 5 for more details.

note here that the detection does not necessarily depend on the line strength. For example, lines such as H β and even H γ in the Be star ζ Tau have line effects of order 1%, while the lines themselves hardly reach above the continuum (see the review by Oudmaijer 2007). The fact that strong lines do not exhibit a line effect is thus a very strong observational finding. Finally, R Mon appears to be an exceptional object in the sense that it is the only star in our sample that has a polarisation effect in most of its emission lines. We will return to this object later in the following discussion.

4 ANALYSIS

The spectropolarimetric results of the sample show a continuum polarisation at the level between $\sim 0.3\%$ to $\sim 12\%$. Unlike the polarised standard stars, the majority of objects do not follow the empirical curve of the Serkowski law. A line effect is present across the H α line in all objects.

We observe three different line effects across the H α line in the sample (see Table 4): depolarisation, intrinsic polarisation; and a polarisation change across the absorption, which is commonly referred to as the McLean effect. In depolarisation, the polarisation across the emis-

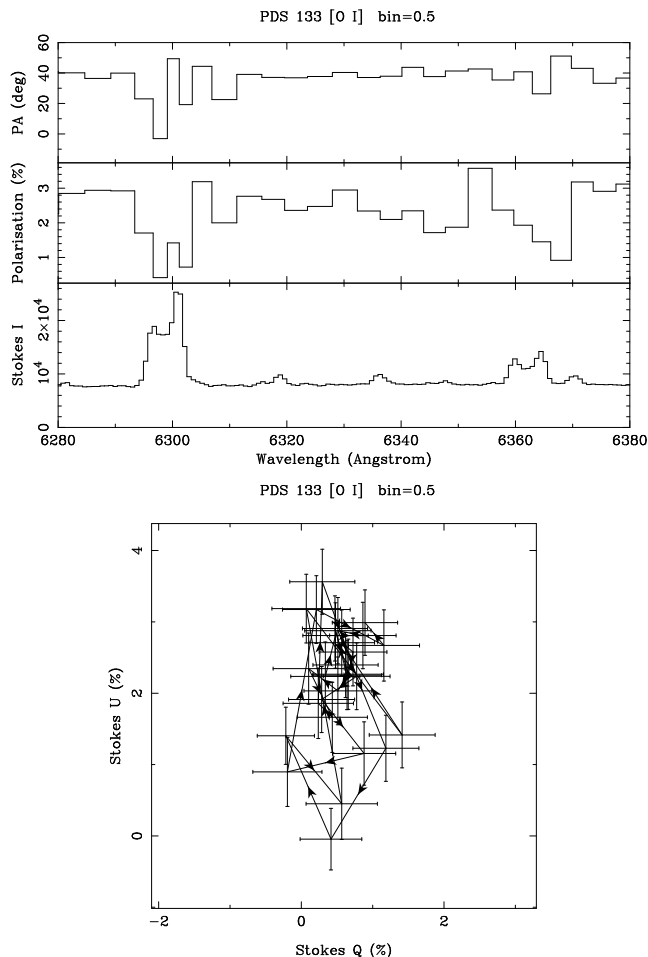


Figure 8. [O I] at 6300 and 6364 Å polarisation data of PDS 133. See the caption of Fig. 5 for more details.

sion line decreases compared to the continuum, and it is more common in high mass stars (Clarke & McLean 1974; Poeckert & Marlborough 1976). Intrinsic line polarisation can be due to an anisotropic line emitting region scattering off circumstellar material, and it was found in T Tauri and HAe stars (Vink et al. 2002, 2003, 2005). The McLean effect is where the absorption component of the emission line often has a different polarisation than the continuum, but the emission has not (McLean 1979). There is a distinct difference in polarimetric properties between the HBe stars, showing de-polarisation and the HAe stars showing enhanced polarisation across the line.

The intrinsic line polarisation is thought to be caused by the effects of magnetospheric accretion. In this case, disk material is funnelled through accretion columns on to the stars. The material shocks the photosphere where it crashes into at high speeds. The line emission coming from these hot spots will be polarised as they scatter off the disk material, which becomes detectable as a line effect (Vink, Harries & Drew 2005).

4.1 McLean effect

A number of objects display a polarisation change across the P Cygni absorption of the hydrogen lines and do not necessarily fit into the categories above.

The concept of the McLean effect is based on the fact that the wind material in our line of sight blocks the unscattered light and removes it from the beam. This leads to observation of a strong emission line with a blueshifted absorption component. However, the flux in the absorption does not reach zero because the re-emission process is isotropic; some of the photons will be scattered into our line of sight. If the distribution of the scattering material is aspherical, the observed light across the absorption will be more polarised than the continuum light. PDS 27, PDS 37 and PDS 133 show a clear McLean effect across the absorptive component of H α . The line effect is of order 1-2% in these objects. Naively, we might expect the same line effect across the H β but this is not observed. Fig. 9 shows the H α and H β P Cygni profile of PDS 27, PDS 37 and PDS 133. The P Cygni absorption seems to be saturated with broad and flat core features for PDS 27 and the absorption is around 0.4 and 0.15 of the continuum level for H α and H β respectively. In PDS 37, the P Cygni absorption is at 0.75 and 0.3 of the continuum level for H α and H β respectively. The absorption in H β is thus deeper than that of H α in both objects. This is not expected as typically the higher lines display weaker absorption. This unusual behaviour is also seen for the Paschen lines as presented in Fig. 10. The figure shows that the absorption component of Pa β is weaker than Pa γ and Pa δ . Unlike PDS 27 and PDS 37 the absorption part of the line of PDS 133 is above the continuum.

By analysing the observed P Cygni spectral lines and the observed polarisation line effects, we can understand the McLean effect in H α and its absence in H β relatively straightforwardly. The strong H α line photons are scattered into the line of sight filling in the absorption component. If the scattering region is a-symmetric, net polarisation across the absorption part of the line will be observable.

The H β line, which is weaker than H α has fewer photons, and will therefore also have fewer scattered photons filling the absorption component (see Fig. 9). The net effect is that both the H β absorption remains deeper than for H α , while the scattered, polarised component is less obvious. Therefore, the lack of the scattered photons in H β could explain the absence of the line effect across this line. This argument is supported by the observed line effects across the absorptive component of H α in PDS 27, PDS 37 and PDS 133, as the line effect is stronger for a weaker absorption component. Ababakr et al. (2015) suggested a similar scenario in an in-depth study of PDS 27 and PDS 37, but here we have an extra object that follows the same pattern.

For illustration, we sketch the situation in Fig. 11. In the schematic we can see that different levels of polarisation in the line of sight result in different absorption line profiles. In the case of large polarisation, we do not see any absorption in the observed line profile as the polarised light fills in the absorption. Interestingly, the McLean effect can thus also be observed in the absence of absorption. In contrast, very deep absorption would be observed when there is little or no polarisation.

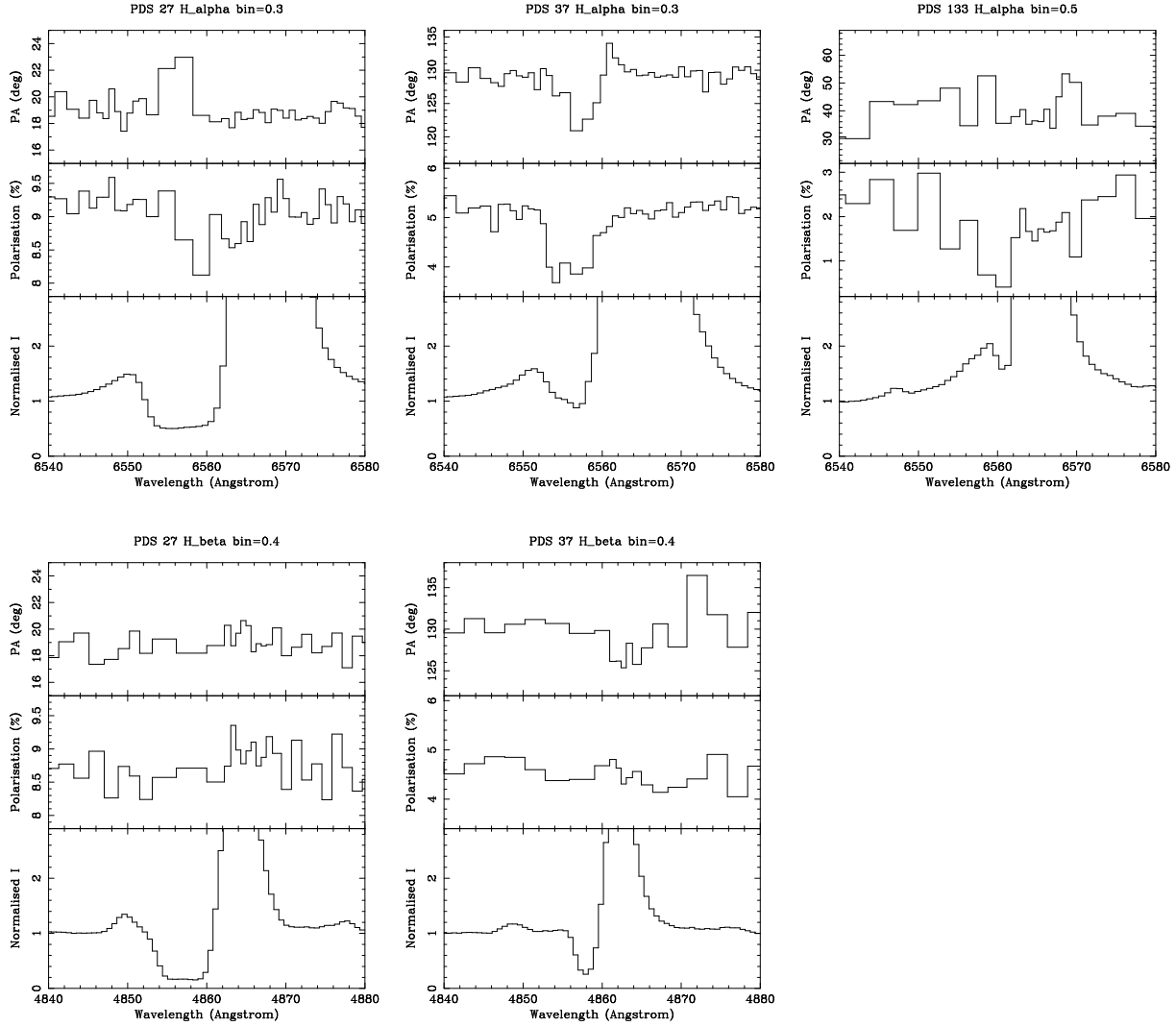


Figure 9. $H\alpha$ and $H\beta$ spectropolarimetry of PDS 27, PDS 37 and PDS 133. For PDS 133 only $H\alpha$ data is available. See the caption of Fig. 5 for more details.

4.2 The case of R Mon

A small number of objects display line effects across more lines than $H\alpha$ alone. We discuss these here, focussing on the most extreme object, R Mon. Its continuum polarisation is large, with values of order 12% and 8%, in the R band in 2012 and 2011 respectively. Unlike the other stars, R Mon displays a line effect across virtually all observed emission lines. The difference between line and continuum polarisation is 7% across the $H\alpha$ and $H\beta$ lines (see Figs. 5 and 6), which is large and rare. Typically, the strongest line effect due to electron scattering is of order 2% (Oudmaijer 2007). In addition, the direction of the intrinsic polarisation angle from the line effects in the (Q, U) diagram is not constant over different bands. Therefore, it would appear that R Mon is atypical as it differs on many counts from most objects that have been studied spectropolarimetrically.

Relevant to this discussion is that R Mon is an extended object. Its reflection nebula is due to radiation from the inner parts, such as the star and wind, being scattered off circumstellar dust particles, resulting in strong polarisation. Spa-

tially resolved polarisation images reveal polarisation in excess of 50 % (Jolin et al. 2010). The polarised flux is largest closest to the star and decreases with distance, while the polarisation angles follow a centro-symmetric pattern. For a circularly symmetric, highly polarised object on the sky, the same would apply, but if it were unresolved, the net observed polarisation would be zero. However, because R Mon is asymmetric, a net polarisation will be observed, and this is even stronger in our data as the scattering circumstellar material is resolved and larger than the slit.

These features have important consequences for the observed polarimetry. Below we will argue that this is the main reason that the (spectro-)polarimetric properties of R Mon are different from the other stars, and that the various emission lines originate from different line forming regions. For example, given that the polarisation drops off rapidly with distance from the star, a slight change in seeing or slight change in the positioning of the slit can result in largely different polarised light entering the slit. In addition, larger positioning errors can result in differently observed position angles, as the PA depends on position.

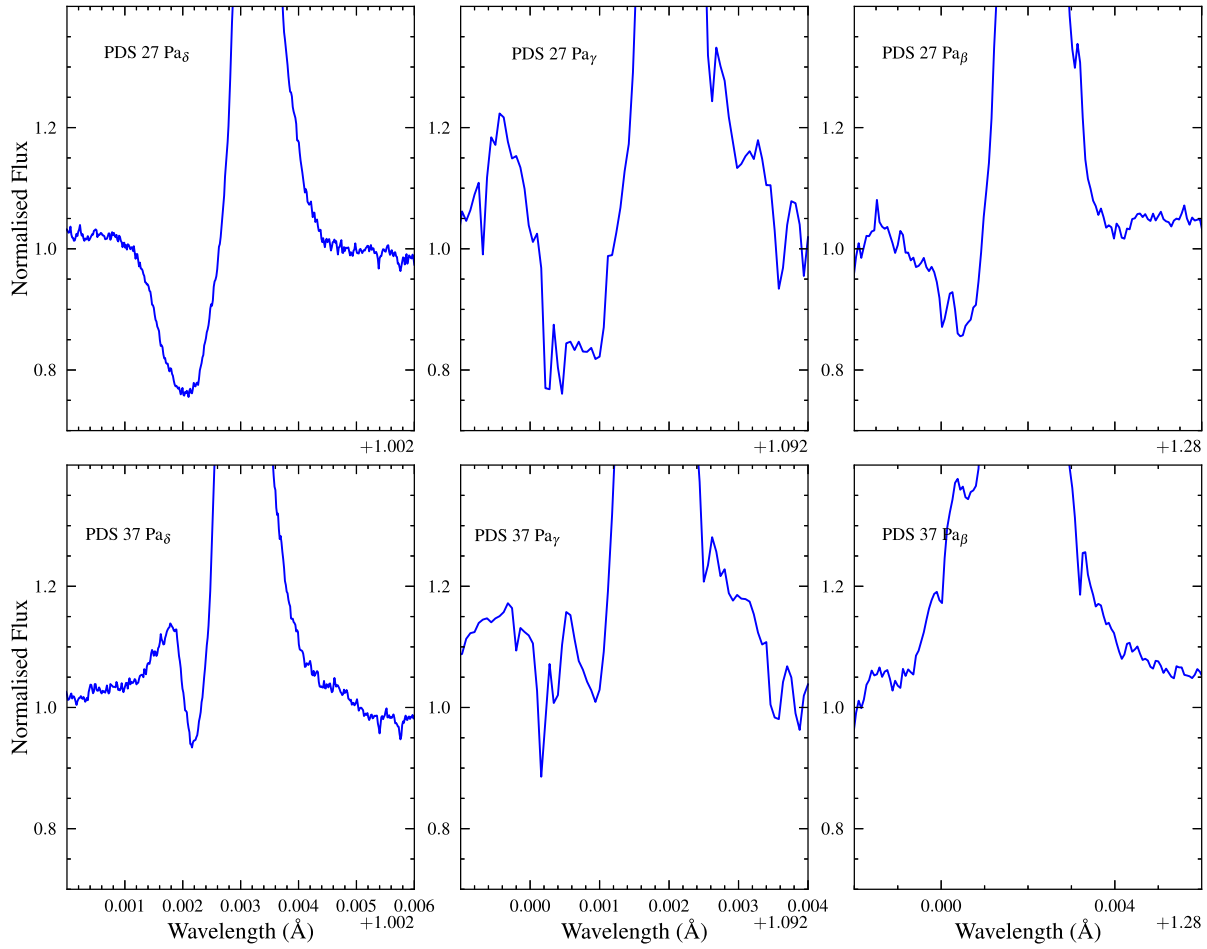


Figure 10. The comparison of P Cygni profile, $\text{Pa}\delta$, $\text{Pa}\gamma$ and $\text{Pa}\beta$ of PDS 27 and PDS 37. The spectroscopic data are taken from the HAeBe X-shooter project (Oudmaijer et al. 2011; Fairlamb et al. 2015)

Inspection of the raw spectropolarimetric data shows that the width of the ordinary (O) and extraordinary (E) beam in the spatial direction in the 2011 data is about twice that of the 2012 data (and wider than the data for the other stars). In addition, the individual beams do not follow the typical Gaussian shape of the seeing profile, but appear asymmetric. This confirms that R Mon is not a point source but an irregular, extended object.

Let us discuss the polarisation properties of R Mon in this context, starting with its observed broadband peculiarities. The polarisation seemingly increased by 4% over a timespan of 4 months, while the polarisation angle stayed the same. The slit direction and position were the same for both observations but as mentioned above, the spatial profile of the 2011 data, which has a smaller level of polarisation, is much wider than that in 2012. As the polarisation closest to the object is highest, it follows that the net polarisation in 2012 is higher. A similar argument can be put forward to explain the discrepant position angles for each of the wavebands the object was observed. In Fig. 4, the slope of the PA is the same for the V , R and I bands, but they are offset by 10° (see also Table 2). According to the data in Jolin et al. (2010), the polarisation is centro-symmetric, and the polarisation angle changes with at least 20° every 1 arc-sec. Hence, a slight displacement can result in a noticeable

change in PA. We argue, therefore, that the fact that R Mon is extended and asymmetric explains the high polarisation, large continuum variability, and offset in PA for the various wavelength settings.

Let us now turn to the spectropolarimetric properties, of which the fact that most lines seem to exhibit a line effect, and that the line effect is large, makes R Mon stand out.

The left hand panel of Fig. 12 shows the (Q, U) diagram of three forbidden lines of R Mon, with each line taken from a different wavelength setting. The right hand panel shows lines from different wavelength settings as well; $\text{H}\beta$, $\text{H}\alpha$ and a Ca II triplet line, at 8662 \AA . The line excursions are large, ranging from $\sim 5\%$ to $\sim 10\%$ in $\text{H}\alpha$. The direction of the intrinsic polarisation angle is roughly the same for all forbidden lines, with an average value of $64 \pm 5^\circ$. However, very different intrinsic angles of $90 \pm 15^\circ$, $57 \pm 10^\circ$ and $128 \pm 10^\circ$ are found for $\text{H}\beta$, $\text{H}\alpha$ and the Ca II triplet line respectively. The $\text{H}\alpha$ and Ca II triplet data were taken at the same date while $\text{H}\beta$ was taken a few days later. The polarisation angle in $\text{H}\alpha$ is the only one consistent with the forbidden lines.

The question that now arises is how can the line effects be strong, and why would the intrinsic angles be different for the various lines? By simply stating that the lines are formed in a larger region than the star and would be less

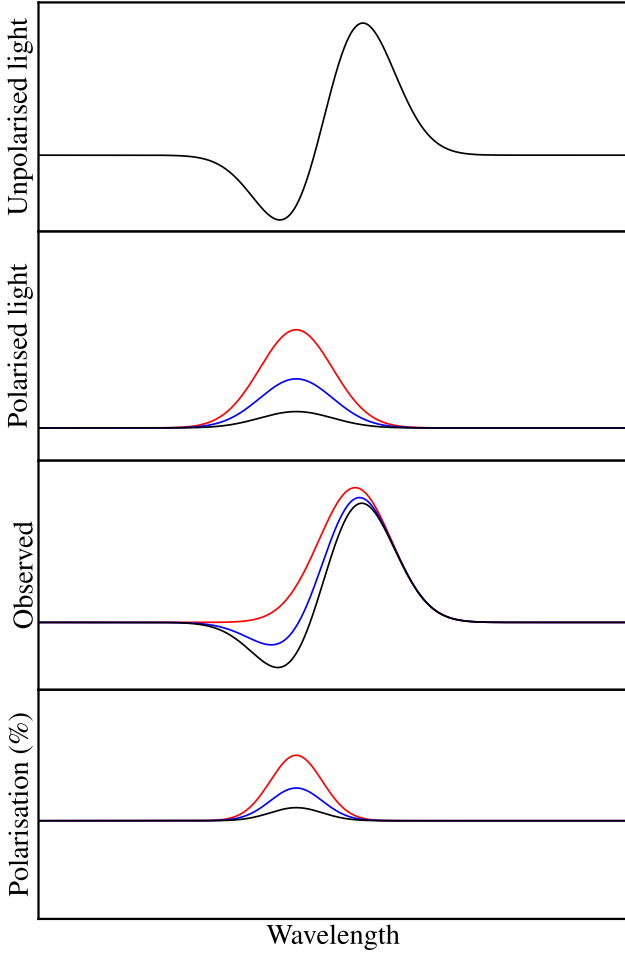


Figure 11. Schematic explaining the McLean effect with the data present in three sets: the unpolarised light is shown in the upper panel, polarised light into the line of sight in the upper middle, the observed $H\alpha$ line profile in the lower middle and the observed polarisation (%) is shown in the lower panel. The absorption is completely filled when there is a significant amount of polarisation in our line of sight, this results in a detection of a notable line effect (red solid line). In contrast, when the polarised light into our line of sight is not sufficient to fill in the absorption component significantly, this results in a weak line effect which is challenging to observe (black solid line). The solid blue line represents an average between the two extreme cases.

prone to scattering, such as the polarisation dilution discussed in Trammell et al. (1994), does not hold in the current situation. The reflecting dust is located far away from the star and is in all likelihood much more extended than the ionized wind. In this case, the emission lines will be equally likely to be scattered and thus as polarised as the continuum. The remaining possibility is that the line emitting regions themselves are not isotropic - either asymmetric or clumpy, leading to a polarisation line emission different from the continuum. The different polarisation angles for the various lines may be the result of different geometries and volumes of the line forming regions. The optically thick $H\alpha$ emission and the forbidden lines originate from large, possibly similar volumes, which could follow similar scattering paths, whereas other lines arise in regions closer to

the star and have potentially different geometries, leading to different polarisation angles.

To our knowledge this is the first time an object has been reported to have so many lines with a polarisation effect across them. It will not be trivial to disentangle the various contributions and multi-parameter modelling is needed to retrieve the geometry of the system. This is beyond the scope of the current paper.

5 FINAL REMARKS AND CONCLUSIONS

We have performed the first linear spectropolarimetry over a large wavelength range of a sample of HAeBe stars. The spectra cover the range from 4560 Å to 9480 Å, including many emission lines such as: hydrogen recombination lines, Ca II, Fe II, O I and He I and several forbidden lines including [O I], [Fe II] and [S II]. All the objects have a measurable continuum polarisation, ranging from $\sim 0.3\%$ in the very low polarised star HD 85567 to $\sim 12\%$ in the highly polarised star R Mon. Our values are broadly consistent with these values but there are some variations from the literature values. The continuum polarisation of some of our objects do not follow the general trend of the Serkowski law. This is evidence of the presence of intrinsic polarisation in the observed continuum polarisation as the interstellar polarisation does not vary significantly over time.

All the objects show a sign of line effect across $H\alpha$. All HBe objects display either a classical depolarisation or a McLean effect signature. The HAe objects show a mixture of McLean, depolarisation, intrinsic line polarisation and complex line effect. This suggests that the circumstellar environments around HAeBe stars have a flattened structure. Four objects in our sample show a McLean effect, where the change in polarisation occurs across the absorptive component of the emission line of $H\alpha$. This suggests that the distribution of the ionised material is not circular on the sky. From these four objects we only have $H\beta$ data for PDS 27 and PDS 37. We would expect the same line effect across the absorption component of $H\beta$. However, the absorption in $H\beta$ is approximately three times stronger than that of $H\alpha$. We can explain this apparent inconsistency by the fact that strong $H\alpha$ line emission scatters into our line of sight filling in the absorption component. The $H\beta$ line is weaker than $H\alpha$ and thus fewer scattered photons fill in the absorption component, yielding a much lower polarisation effect, consistent with the observed non-detection.

It would appear, therefore, that we can explain the differing polarisation behaviour across the absorption parts of the $H\alpha$ and $H\beta$ lines very well in the context of the McLean effect. An alternative scenario to explain polarisation across the absorption parts of hydrogen lines was put forward by Kuhn et al. (2007). Essentially this invokes selective optical pumping of the lines, predicting that both $H\beta$ and $H\alpha$ will have polarisation effects of roughly similar magnitude (Kuhn et al. 2011, their Figs. 4 and 5). This is not what we observe in our data. What is more, this scenario will also struggle to explain why the $H\beta$ absorption is so much stronger than that of $H\alpha$. Within the current set of observations, the McLean effect seems to be a more viable explanation.

Four HBe objects show a depolarisation line effect,

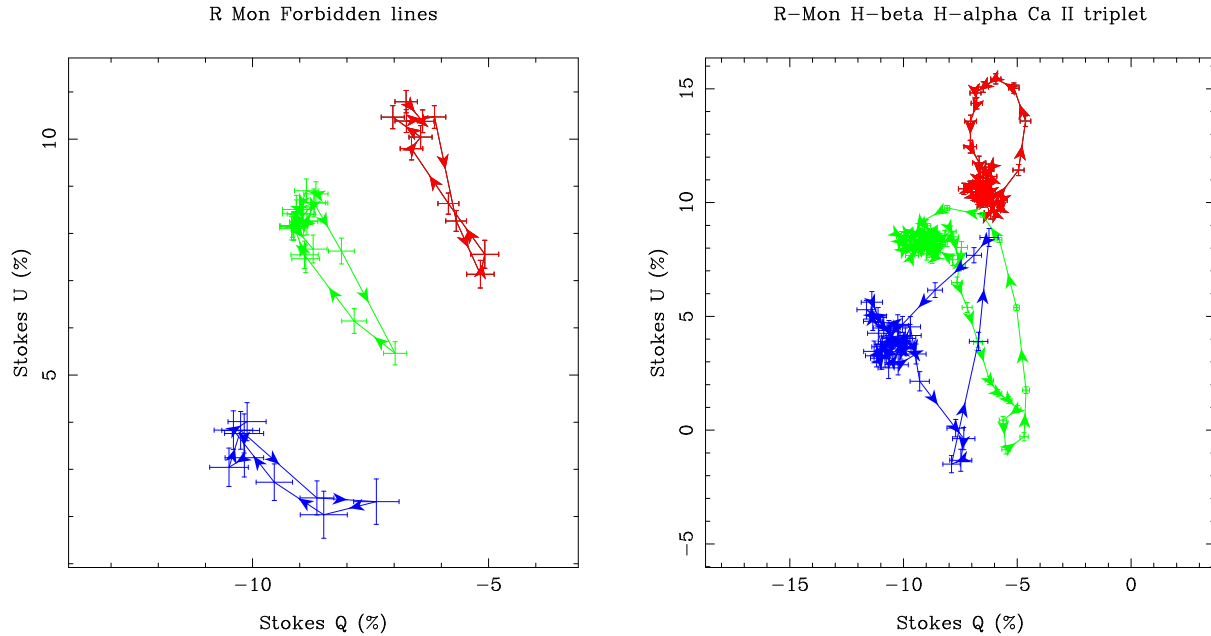


Figure 12. (Q , U) diagram of several spectral lines and forbidden lines of R Mon. The lines are taken from B band (blue solid line), R band (green solid line) and I band (red solid line). $H\beta$, $H\alpha$ and $Ca II$ triplet at 8662 Å are presented in blue, green and red lines respectively (right); three forbidden lines: $[Fe II]$ at 5158 Å, $[O I]$ at 6364 Å and $[Fe II]$ at 8616 Å are shown in blue, green and red lines respectively (left).

where the change in polarisation is as broad as the emission line. This suggests that $H\alpha$ emerge in an extended circumstellar disk. Two H Ae objects show an intrinsic line polarisation, where a significant portion of the photons emerge from accretion hot spots. BF Ori and HD 104237 show a possible line effect across $H\alpha$.

We have observed depolarisation line effects across $[O I]$ lines at 6300 and 6364 Å in PDS 133, R Mon and CPD-485215. The line profile in PDS 133 is broad and double peaked unlike the other two, which are narrow and single peaked. The line profiles may suggest that the lines originate from a rotating disk in PDS 133 while in R Mon and CPD-485215 many forbidden lines display a depolarisation line effect. It is to be expected to see a depolarisation line effect across $[O I]$ in PDS 133 as they originate in the disk further out from the inner ionised disk. The $Ca II$ triplet also shows a depolarisation in MWC 275. These lines have low ionisation potential energy as they are formed in a predominantly neutral zone. In general they originate in the circumstellar environment but outside the hydrogen ionisation boundary. Therefore, we might expect a depolarisation line effect across these lines. However, for the objects that display a depolarisation line effect, the $Ca II$ triplet line effects are either absent or very weak.

Finally, we have presented the medium resolution spectropolarimetry on the entire optical range from 4560 Å to 9480 Å of a sample of 12 HAeBe stars. The data allow us to draw the following conclusions:

- We sample linear line spectropolarimetry in the optical wavelength range, which is much larger than any previous work at similar spectral resolution.
- Changes in the polarisation across the $H\alpha$ emission line are detected in all objects, as an indication of a flattened

structure of the circumstellar environment. The line effects vary from depolarisation, line polarisation to the McLean effect.

- Depolarisation and the McLean effect are observed in Be type stars predominantly in early B type stars while line polarisation is observed in Ae type objects.
- The McLean effect is observed only across the absorptive component of $H\alpha$ and the line effect is stronger for a weaker absorption component, while $H\beta$ does not display the effect. We propose a scenario to explain this property. It is based on the fact that the photons from the strong $H\alpha$ line are scattered into the line of sight. As a consequence, the photons in the absorption are more polarised than the emission. A side result is that the selective absorption due to optical pumping as proposed by Kuhn et al. (2007) is unlikely to be responsible for the polarisation behaviour in these objects.
- We detect a broad depolarisation line effect across $Ca II$ triplet and $[O I]$ in two objects. These lines are emerging further away from the star and $H\alpha$ region in the circumstellar environment. The depolarisation simply implies that the circumstellar environment has an asymmetrical structure in this region.
- The few spectra with calcium triplet lines that show an effect show a similar polarisation profile for all members of the triplet. We confirm a similar observation by Kuhn et al. (2011) for an evolved, RV Tau star. As these authors explained, resonant line scattering can then not be the cause for the observed line polarisation, as the $Ca II$ 8662 Å comes from a different upper level than the other members of the triplet. Similar polarisation due to line scattering would then not be expected.
- Finally, apart from $H\alpha$, few lines in few objects show a line effect in the polarisation. We present the case of R Mon,

which displays exceptionally strong line effects in most of its emission lines. In addition, not all lines show the same type of line effect. We explain this by the fact that the object itself is resolved and propose that different line forming regions and geometries are responsible for polarisation properties of the higher hydrogen recombination lines and forbidden lines and H α on the other hand.

ACKNOWLEDGEMENTS

We are very grateful to the referee, Richard Ignace, for his constructive and very insightful remarks that helped us improve the paper. This research has made use of the SIMBAD database, operated at CDS, Strasbourg, France.

REFERENCES

- Ababakr K. M., Fairlamb J. R., Oudmaijer R. D., van den Ancker M. E., 2015, *MNRAS*, 452, 2566
- Acke B., van den Ancker M. E., Dullemond C. P., 2005, *A&A*, 436, 209
- Beltrán M. T., de Wit W. J., 2016, *A&A Rev.*, 24, 6
- Clarke D., McLean I. S., 1974, *MNRAS*, 167, 27P
- Fairlamb J. R., Oudmaijer R. D., Mendigutía I., Ilee J. D., van den Ancker M. E., 2015, *MNRAS*, 453, 976
- Fossati L., Bagnulo S., Mason E., Landi Degl’Innocenti E., 2007, in Sterken C., ed., *The Future of Photometric, Spectrophotometric and Polarimetric Standardization Vol. 364 of Astronomical Society of the Pacific Conference Series, Standard Stars for Linear Polarization Observed with FORS1*. p. 503
- Grady C., Fukagawa M., Maruta Y., Ohta Y., Wisniewski J., Hashimoto J., Okamoto Y., Momose et al., 2015, *Ap&SS*, 355, 253
- Grinin V. P., 1994, in The P. S., Perez M. R., van den Heuvel E. P. J., eds, *The Nature and Evolutionary Status of Herbig Ae/Be Stars Vol. 62 of Astronomical Society of the Pacific Conference Series, Polarimetric activity of Herbig Ae/Be stars*. p. 63
- Harries T. J., 1996, *Starlink User Note*, 204
- Herbig G. H., 1960, *ApJS*, 4, 337
- Hillenbrand L. A., Strom S. E., Vrba F. J., Keene J., 1992, *ApJ*, 397, 613
- Ignace R., Brimeyer A., 2006, *MNRAS*, 371, 343
- Ilee J. D., Fairlamb J., Oudmaijer R. D., Mendigutía I., van den Ancker M. E., Kraus S., Wheelwright H. E., 2014, *MNRAS*, 445, 3723
- Jain S. K., Bhatt H. C., 1995, *A&AS*, 111, 399
- Jolin M.-A., Bastien P., Denni F., Lafrenière D., Doyon R., Voyer P., 2010, *ApJ*, 721, 1748
- Kraus S., 2015, *Ap&SS*, 357, 97
- Kuhn J. R., Berdyugina S. V., Fluri D. M., Harrington D. M., Stenflo J. O., 2007, *ApJL*, 668, L63
- Kuhn J. R., Geiss B., Harrington D. M., 2011, in Kuhn J. R., Harrington D. M., Lin H., Berdyugina S. V., Trujillo-Bueno J., Keil S. L., Rimmele T., eds, *Solar Polarization 6 Vol. 437 of Astronomical Society of the Pacific Conference Series, Using Absorptive Linear Polarization Spectroscopy to Understand Imbedded Stars*. p. 245
- McLean I. S., 1979, *MNRAS*, 186, 265
- Mottram J. C., Vink J. S., Oudmaijer R. D., Patel M., 2007, *MNRAS*, 377, 1363
- Muzerolle J., Calvet N., Hartmann L., 1998, *ApJ*, 492, 743
- Oudmaijer R. D., 2007, in Hartquist T. W., Falle S. A. E. G., Pittard J. M., eds, *Diffuse Matter From Star Forming Regions to Active Galaxies*. Springer-Verlag, Berlin, p. 83
- Oudmaijer R. D., Drew J. E., 1999, *MNRAS*, 305, 166
- Oudmaijer R. D., Palacios J., Eiroa C., Davies J. K., de Winter D., et al., 2001, *A&A*, 379, 564
- Oudmaijer R. D., Proga D., Drew J. E., de Winter D., 1998, *MNRAS*, 300, 170
- Oudmaijer R. D., van den Ancker M. E., Baines D., Caselli P., Drew J. E., Hoare M. G., Lumsden S. L., Montesinos B., Sim S., Vink J. S., Wheelwright H. E., de Wit W. J., 2011, *Astronomische Nachrichten*, 332, 238
- Poeckert R., Marlborough J. M., 1976, *ApJ*, 206, 182
- Quirrenbach A., Buscher D. F., Mozurkewich D., Hummel C. A., Armstrong J. T., 1994, *A&A*, 283, L13
- Rodrigues C. V., Sartori M. J., Gregorio-Hetem J., Magalhães A. M., 2009, *ApJ*, 698, 2031
- Serkowski K., Mathewson D. S., Ford V. L., 1975, *ApJ*, 196, 261
- The P. S., de Winter D., Perez M. R., 1994, *A&AS*, 104, 315
- Tody D., 1993, in Hanisch R. J., Brissenden R. J. V., Barnes J., eds, *Astronomical Data Analysis Software and Systems II Vol. 52 of Astronomical Society of the Pacific Conference Series, IRAF in the Nineties*. p. 173
- Trammell S. R., Dinerstein H. L., Goodrich R. W., 1994, *ApJ*, 108, 984
- Vieira S. L. A., Corradi W. J. B., Alencar S. H. P., Mendes L. T. S., Torres C. A. O., Quast G. R., Guimarães M. M., da Silva L., 2003, *ApJ*, 126, 2971
- Vink J. S., 2015, *Ap&SS*, 357, 98
- Vink J. S., Drew J. E., Harries T. J., Oudmaijer R. D., 2002, *MNRAS*, 337, 356
- Vink J. S., Drew J. E., Harries T. J., Oudmaijer R. D., Unruh Y., 2005, *MNRAS*, 359, 1049
- Vink J. S., Drew J. E., Harries T. J., Oudmaijer R. D., Unruh Y. C., 2003, *A&A*, 406, 703
- Vink J. S., Harries T. J., Drew J. E., 2005, *A&A*, 430, 213
- Vrba F. J., Schmidt G. D., Hintzen P. M., 1979, *ApJ*, 227, 185
- Wheelwright H. E., Bjorkman J. E., Oudmaijer R. D., Carciofi A. C., Bjorkman K. S., Porter J. M., 2012, *MNRAS*, 423, L11
- Wheelwright H. E., Vink J. S., Oudmaijer R. D., Drew J. E., 2011, *A&A*, 532, A28
- Whittet D. C. B., Martin P. G., Hough J. H., Rouse M. F., Bailey J. A., Axon D. J., 1992, *ApJ*, 386, 562
- Yudin R. V., Evans A., 1998, *A&AS*, 131, 401

APPENDIX A: OBSERVED POLARISATION IN THE OPTICAL RANGE FROM ~ 4600 Å TO ~ 9400 Å FOR ALL OBJECTS

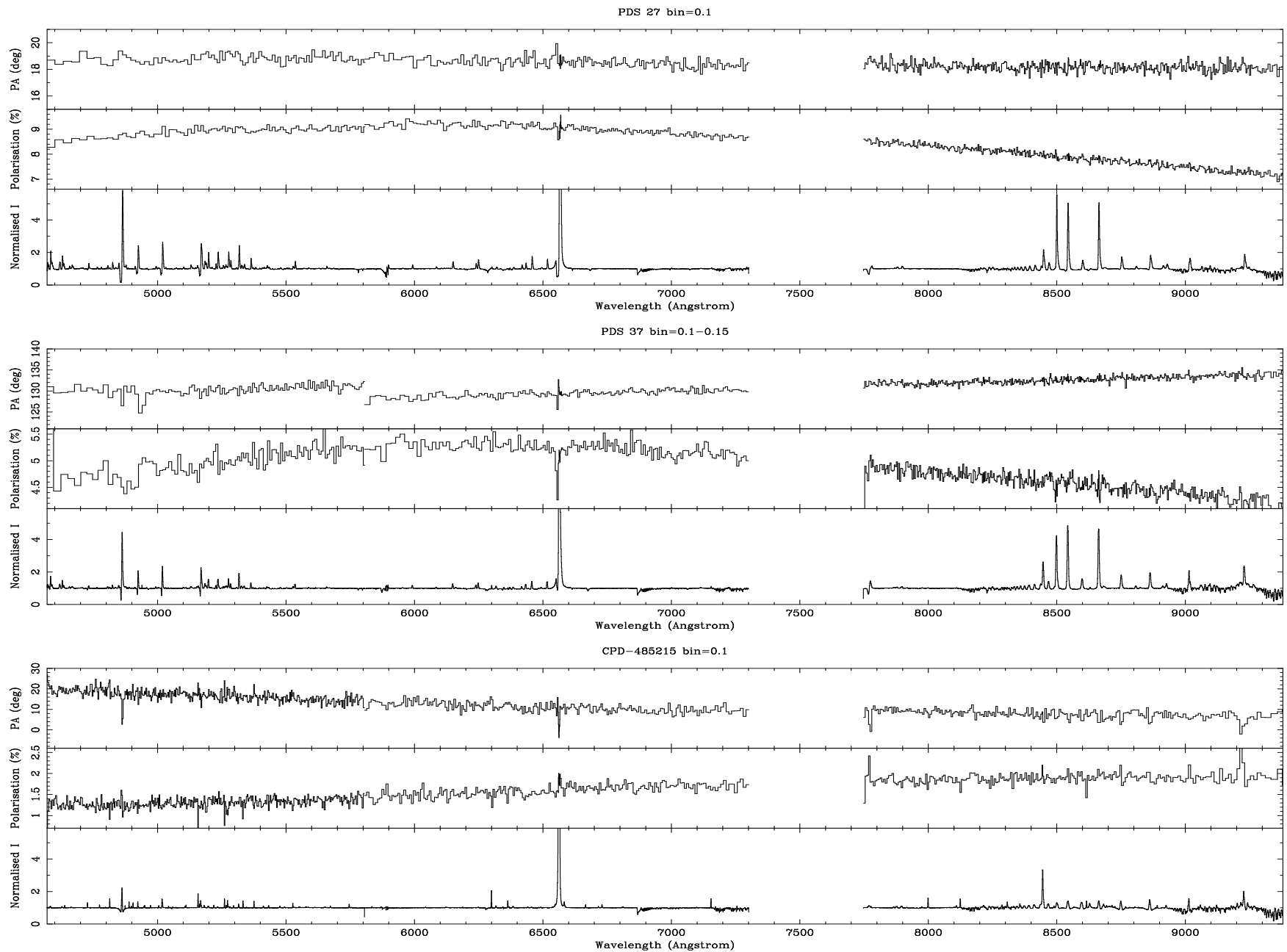


Figure A1. The polarisation data in *V*, *R* and *Z* bands for PDS 27, PDS 37, CPD-485215, R Mon and V380 Ori; and in *R* and *Z* bands for GU CMa, HD 98922, PDS 133, HD 104237, MWC 275, BF Ori and HD 85567. R Mon, V380 Ori and HD 85567 are presented in two epochs in *R*. The data are presented as a triplots. In the triplot polarisation spectra the Stokes intensity (*I*) is shown in the lower panel, polarisation (%) in the centre, while the position angle (PA) is shown in the upper panel. The data are rebinned to a constant value, as indicated at the top of each plot.

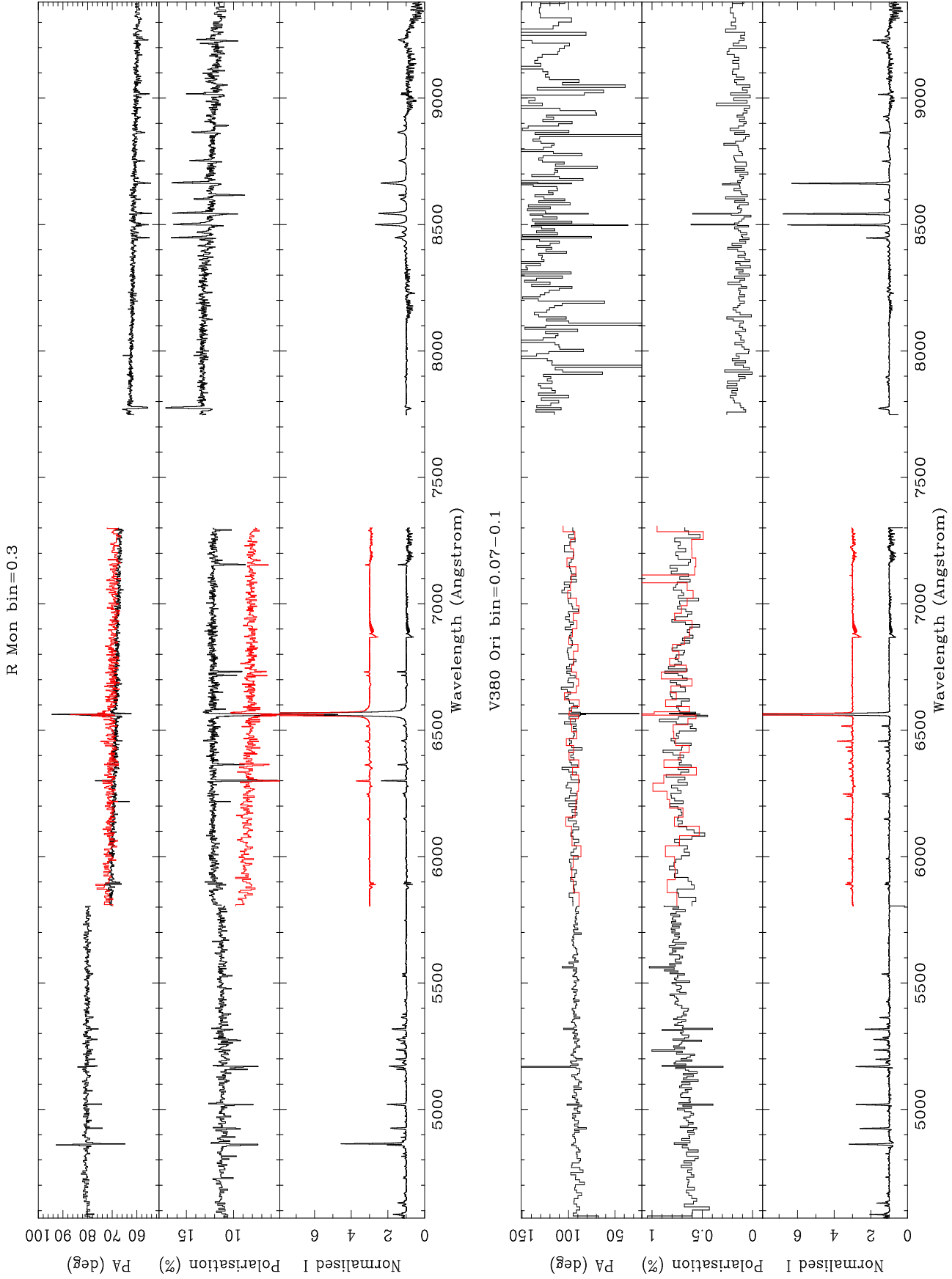


Figure A1. continued

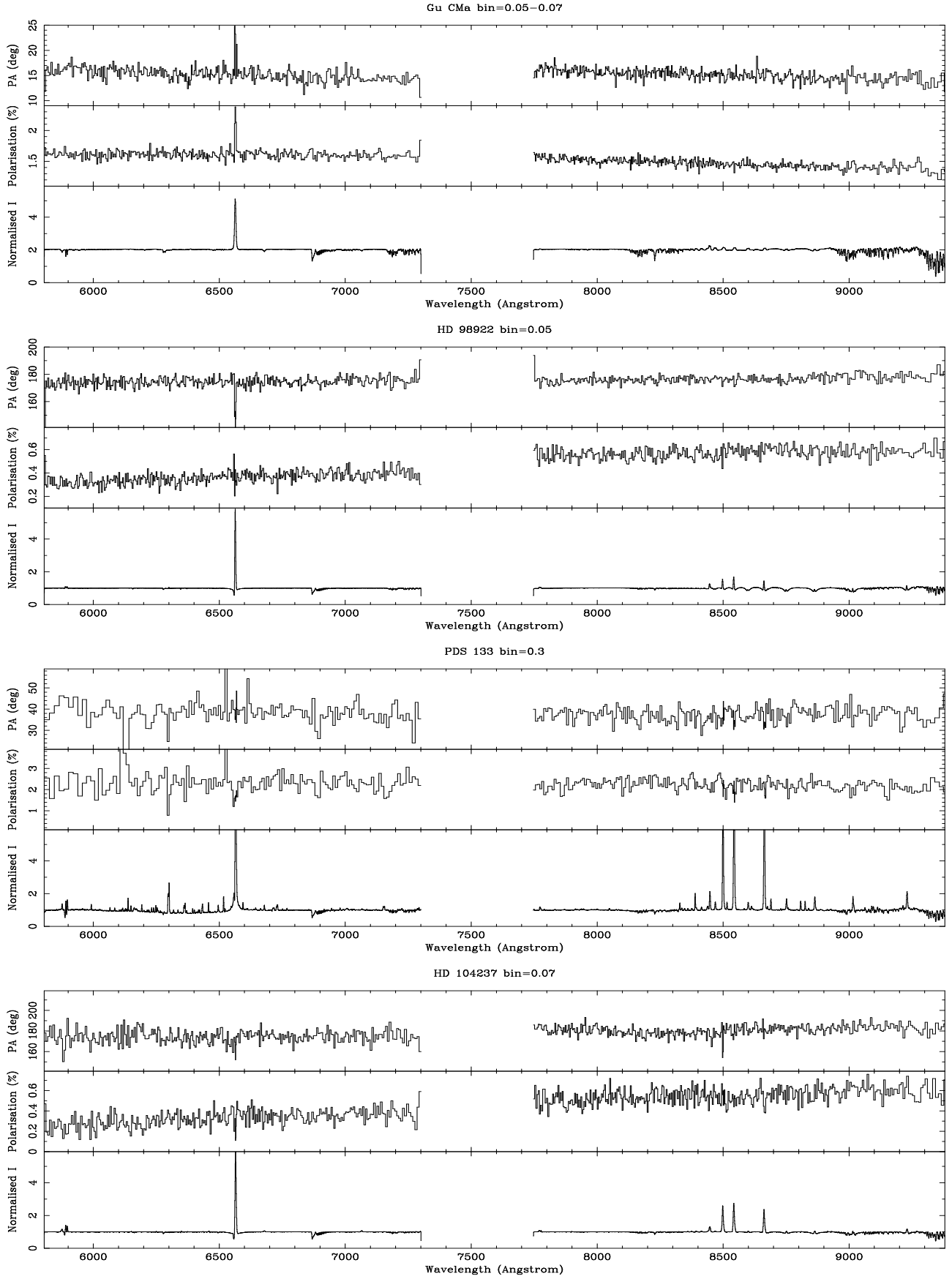


Figure A1. continued

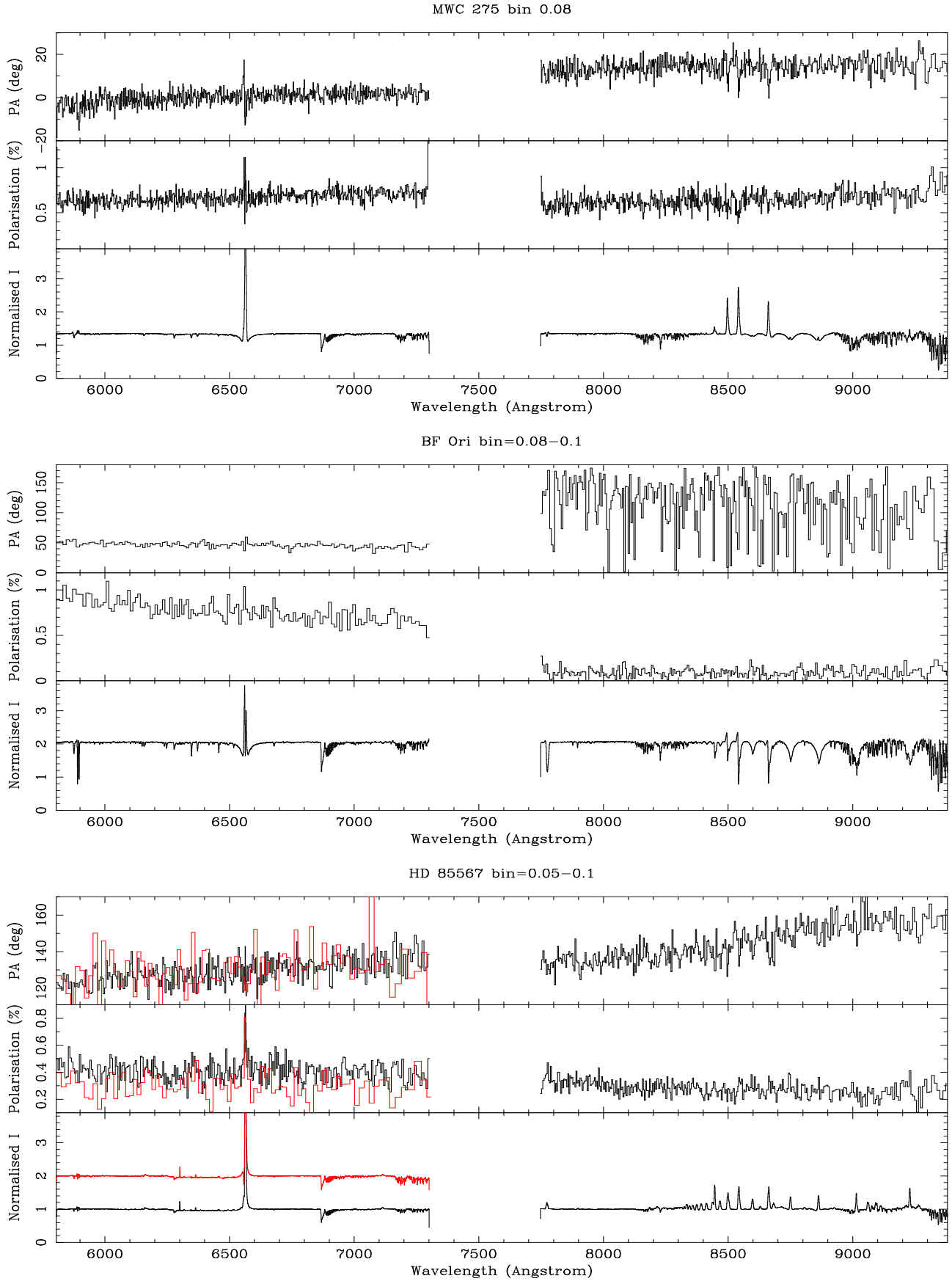


Figure A1. continued